

Quantum circuit model for Hamiltonian simulation via Trotter decomposition

Rohit Sarma Sarkar,^{*} Sabyasachi Chakraborty,[†] and Bibhas Adhikari[‡]

Abstract. We devise quantum circuit implementation of exponential of scaled n -qubit Pauli-strings using one-qubit rotation gates and CNOT gates. These circuits can be implemented in low-connected quantum hardware, in particular, star graph architecture for digital quantum computation. Then these circuits are employed to simulate classes of 1D Hamiltonian operators that include 2-sparse Hamiltonian, Ising Hamiltonian, and both time-independent and time-dependent Random Field Heisenberg Hamiltonian and Transverse Magnetic Random Quantum Ising Hamiltonian by approximating its unitary evolution with first-order Suzuki-Trotter expansion. Finally, we perform noisy Hamiltonian simulation of these circuits using different noise models to investigate Hamiltonian simulation on NISQ devices.

Keywords. Hamiltonian, quantum circuits, Suzuki-Trotter product formula

1 Introduction

Quantum circuit model offers the promise for simulation of quantum dynamics of many-body systems in near-term with digital quantum computers [17]. In particular, quantum neural networks defined by parametrized quantum circuits provide a suitable platform for implementing learning algorithms for parametrized Hamiltonian learning [65] [56]. Seeking quantum advantage for real world applications, methods are proposed to formulate optimization problems as ground-state finding problem for a Hamiltonian of a many-body physical system associated with the objective or loss function of the optimization problem [6]. Thus, designing quantum circuits that can implement the quantum evolution of a given Hamiltonian has become one of the core issues in the practical use of near-term quantum computers such as Noisy Intermediate Scale Quantum (NISQ) devices.

From a physics perspective, the underlying architecture of quantum correlations among units within a physical system is delineated by local interactions among qubits, encapsulated by a local Hamiltonian. This local Hamiltonian ultimately defines the total Hamiltonian of the system. For example, total Hamiltonians governing non-equilibrium phases of matter [28], [23], strongly correlated systems [45], and chemical reaction mechanisms [40], [31] are expressed as linear combinations of Pauli-strings, which encode the local dynamics of the system. Since quantum evolutions are described by unitary matrices for finite-dimensional systems, devising quantum circuits to implement these unitary matrices using universal quantum gates and analyzing the noise in efficiently implementing these circuits in quantum hardware presents one of the key challenges in achieving quantum advantage.

^{*}Department of Mathematics, IIT Kharagpur, India, E-mail: rohit15sarkar@yahoo.com

[†]Department of Physics, IIT Kharagpur, India, E-mail: sabyasachi.sch@gmail.com

[‡]Corresponding author, Fujitsu Research of America, Inc., Santa Clara, USA, E-mail: badhikari@fujitsu.com

Total Hamiltonian of a many-body system is described by

$$H(t) = \sum_{j=1}^L a_j(t) H_j, \quad (1)$$

where H_j is a particular Pauli-string of the total Hamiltonian with associated time dependent coefficient $a_j(t)$, a real valued function of the parameter t , which denotes time. The evolution of the system is governed by the Schrödinger equation $\hbar |\dot{\psi}(t)\rangle = -\iota H(t) |\psi(t)\rangle$, $t \in [0, T]$, where $T > 0$ is the total evolution time, $\iota = \sqrt{-1}$ and \hbar is the Planck constant. If $a_j(t)$ is constant i.e. independent of time parameter t for all j , then the total Hamiltonian is time-independent Hamiltonian, otherwise it is called time-dependent Hamiltonian. The circuit simulation of a Hamiltonian is concerned with the implementation of unitary time evolution $U(t) = \exp(-\iota t H)$ (assuming t to be a unit of \hbar) through a quantum circuit for time-independent case and $U(t) = \mathcal{T} \exp(-\iota \int_0^t H(t') dt')$ for time-dependent Hamiltonian operators, where \mathcal{T} denotes a time-ordering [47].

In this paper, we develop a quantum circuit model for simulating classes of both time-independent and time-dependent 1D Hamiltonian operators employing the first-order Suzuki-Trotter formula for approximating $U(t)$ through product of exponential of local Hamiltonian operators that are Pauli-strings. Thus implementation of exponential of Pauli-strings plays an important role in the simulation, which makes it suitable for implementation of the proposed circuits in digital quantum computers. We develop scalable circuit for exponential of any scaled Pauli-string after determining a permutation similarity of Pauli-strings containing only X gate and the identity matrix. Such a permutation matrix can be implemented in a quantum circuit comprising only a sequence of $\text{CNOT}_{n,j}$ gates in an n -qubit system, $j < n$ follows from our earlier work [55]. We show that a total of at most $2n$ CNOT gates, and at most $(2n - 2)$ one-qubit gates viz. $S = R_Z(\pi/4)$ and H gates i.e. at most $4(n - 1)$ R_Z gates and $2(n - 1)$ R_Y gates are required to implement exponential of an n -qubit Pauli-string. Thus the proposed circuit model favours a quantum hardware with a star architecture in which it is easy to implement these controlled gates with the n -th qubit lies in the center such as IBM Q5 Yorktown/IBM QX2 quantum architecture for 5 qubits [14]. Consequently, the proposed model does not require a fully connected quantum hardware.

We implement the proposed quantum circuit models for simulation of several 1D Hamiltonian operators that include 2-sparse block-diagonal Hamiltonian, Quantum Ising model Hamiltonian, Heisenberg Hamiltonian with random field [46], and Transverse magnetic field quantum Ising model with an external random field [46]. The implementation of these unitary evolution is executed in Qiskit, and we compute the error of approximation for the exact unitary matrix and the proposed circuit model given by the Frobenius norm distance for up to 14 qubits. We notice that the errors in the circuit simulation align with the numerical Trotter approximation errors. Moreover we show that the 1-sparse Hamiltonian and 2-sparse Ising Hamiltonian simulation can be performed with constant circuit depth using the proposed method in this paper.

Finally, we perform noisy simulation of the circuit for various noise models and inputs for the circuits to investigate the performance of the circuit simulation for these Hamiltonian operators in a NISQ like environment. We report the fidelity $\mathcal{F}(t)$ of outputs obtained by noisy and noiseless simulation for time-independent random Field Heisenberg Hamiltonian and transverse magnetic random quantum Ising Hamiltonian for different input states considering three ranges of gate error, which includes bit-flip and phase-flip errors, and idle error, which includes amplitude-damping and phase damping error [42]. These simulations demonstrate that the value of $1 - \mathcal{F}(t)$ remains under 10^{-5} for all t in the interval $[0, 1]$ when the magnitude of gate error and idle error remains below 10^{-3} regardless of the input state during the time evolution. However, when the magnitude of gate error

and idle error ranges between 10^{-3} to 10^{-1} , the fidelity $\mathcal{F}(t)$ of output states drops down to the 0.8 mark during the end of the time evolution for certain states. It is also noteworthy that during the initial stages of the evolution i.e. when t is near 0, the $1 - \mathcal{F}(t)$ remains less than 10^{-4} regardless of the input states. For other ranges of error magnitudes, the fidelity of output states drops below 0.8 for specific input states. Additionally, we observe that the choice of input state is crucial during noisy simulations as greater number of non-zero elements in the input state vector is observed to be a major factor in such drops of fidelity i.e. the input state with more number of zeros will be less effected by noisy quantum circuits during time evolution.

The rest of the paper is organized as follows. Section 2 is devoted to outline the previous work on quantum circuit models for Hamiltonian simulation in the literature. In Section 3, we list the details of the 1D Hamiltonian operators that are considered for testing out the proposed quantum circuit design of exponential of Pauli-strings, given in Section 4. We also briefly review the first-order Trotterization approximation of unitary quantum dynamics for Hamiltonian operators along with the noise models for quantum gates that we consider in this paper. In Section 5, we report the simulation results with empirical approximation errors performed in Qiskit for up to 14-qubit systems. Finally, in Section 6, we compare the noisy and noiseless circuit simulation of time-independent transverse magnetic random quantum Ising Hamiltonian and Random Field Heisenberg Hamiltonian.

2 Related work in the literature

In the literature, various methods are proposed to perform simulation of a quantum many-body Hamiltonian with innovative tools for analyzing the simulation errors. These studies can be divided broadly into two categories based on the proposed techniques. Firstly, methods are developed exploiting the underlying feature of local interactions, such as utilizing the sparsity pattern of the Hamiltonian, among the qubits to estimate the quantum state $|\psi(t)\rangle = U(t)|\psi(0)\rangle$, $t \in (0, T]$ through quantum algorithms that are polynomial in n and T up to a given error tolerance $\epsilon > 0$ [21] [5] [36] [37] [35]. Here $|\psi(0)\rangle$ is the initial state of the n -qubit system. In another approach, product formulae such as Suzuki-Trotter product formulae [62] [60] [61] are employed to approximate $U(t)$ through exponential of local Hamiltonian with or without incorporating the local interaction geometry of the qubits, and then quantum circuit models are developed to estimate $|\psi(t)\rangle$ up to certain empirical error bounds. However, implementation of $U(t)$ through linear combinations of unitary operations rather than products of unitary operations is shown to be more efficient in certain cases [12]. Other approaches such as variational techniques [66] [68] [3], truncated Taylor series [5] [32], truncated Dyson series [26], density matrix exponentiation [27], randomized evolution [9] [16], perturbative quantum simulation [59], using quantum approximate optimization algorithm (QAOA) [34], include some of the distinct techniques introduced for Hamiltonian simulation.

Though product formulae using Trotterization techniques for approximating quantum evolution of a Hamiltonian have poor error scaling [11], tighter error bounds are analytically established for specific types of systems, such as lattice Hamiltonian with nearest-neighbour interactions [11], [10] confirming the empirical error estimates. Strategies for mitigating algorithmic errors due to Trotterized time evolution are investigated through the use of standard polynomial interpolation techniques [52]. Numerical analyses have shown that these product formulae require significantly fewer entangling gates and T gates in the corresponding quantum circuit models compared to the other improved techniques [11], [8].

Indeed, a straightforward implementation of the Suzuki-Trotter type product formula through a quantum circuit has the problem of the use of huge number of gates in the desired quantum circuit (see Section 3.2). Thus reducing the gate count has been one of the primary issues in circuit

simulation of Hamiltonian operators. In [7], the author proposes a method called qDRIFT as a remedy for the scalability issue by introducing an approach leveraging randomization. Besides, the error of approximation using a product formula arise from non-commutative Pauli-strings in the Hamiltonian operator which was later used by [41] in conjunction with partitioning Hamiltonian into commuting Pauli clusters. Thus, partitioning the Pauli-strings into commutative and non-commutative clusters and exploiting these clusters into designing quantum circuits with low depth quantum circuits have been explored in the literature [50] [63] [13] [32] [44] [19] [30] [1].

In another approach, Variational Quantum Algorithms (VQAs) are often regarded as promising for near-term quantum advantage, yet recent research indicates that noise can significantly hinder the trainability of VQAs [64] [58]. Consequently, implementing methods like those proposed by Yao et al. [66] for Hamiltonian operators for large-scale systems in NISQ environments remains challenging. To showcase various attempts in the literature for circuit model of Hamiltonian simulation utilizing Pauli-strings, we display a list of Hamiltonian operators, primary tools for their simulation, and maximum number of qubits for the simulation in Table 1. However, most of these approaches are not scalable and require full connectivity in quantum hardware for implementation, see Table 2.

Ref.	Hamiltonian operators	Tools	Maximum # of qubits
[50]	Kitaev’s honeycomb model BCS Hamiltonian	Checking Parity qubits, Identifying commutative Pauli clusters	10 (experiment), Extrapolated to 100
[63]	Fermionic many-body Hamiltonians, Molecular Hamiltonian (eg. LiH)	Synthesizing circuits for Clifford operators that diagonalize cluster of commutative Pauli-strings	20 (complete result), 48 (incomplete result)
[13]	2D spin Fermi-Hubbard model on 5×5 lattice	“one-layer below” quantum subcircuit	50 (10% accuracy)
[41]	1D Heisenberg Model, LIH (STO 3G basis), H_2 Hamiltonian	Greedy algorithm to partition Hamiltonians into commuting Pauli clusters supported by qDrift	6
[44]	1D Heisenberg Model	Circuit compression using Young-Baxter equation	10
[38]	1D Heisenberg Model, Randomly generated Hamiltonian	Standard and Inverted staircase algorithm	2 5
[67]	Molecular systems	Using quantum circuits for Fermionic excitations	-

Table 1: Circuit models for Hamiltonian simulation in the literature

3 Hamiltonian operators and first-order Suzuki-Trotter expansion

In this section, first we discuss the details of Hamiltonian operators considered in this paper for their circuit simulation, and then we review the first-order Trotterization approximation of unitary dynamics driven by Hamiltonian operators.

3.1 Hamiltonian operators and their structural properties

In this paper, we implement the proposed circuit simulation method for certain time-independent and time-dependent Hamiltonian operators defined on chains of spin-1/2 particles, expressed in terms of the Pauli spin-1/2 matrices given by

$$X = \begin{bmatrix} 0 & 1 \\ 1 & 0 \end{bmatrix}, Y = \begin{bmatrix} 0 & -i \\ i & 0 \end{bmatrix}, Z = \begin{bmatrix} 1 & 0 \\ 0 & -1 \end{bmatrix}$$

and the identity matrix I_2 . The Hamiltonian operators are written as linear combination of Kronecker product of Pauli matrices and their sparsity structure plays an important role during Hamiltonian simulation. We consider a matrix to be k -sparse if each row and column has at most k non-zero entries. Obviously, Pauli-strings are 1-sparse Hermitian unitary matrices.

We consider 2-sparse Hamiltonian operators that correspond to a 2×2 block-diagonal unitary matrix followed by the standard quantum Ising model, the Heisenberg Hamiltonian with a random magnetic field, and the Transverse magnetic field quantum Ising model with an external random field. It is of note that the later two Hamiltonian operators are not exactly solvable [39]. These Hamiltonian operators serve as nice diverse examples to test out our methods which shall be discussed later.

1. The 2-sparse block-diagonal matrices for the Hamiltonian operators are of the form

$$\mathcal{H}_{\text{BLKDG}} = \sum_{\sigma_\alpha \in \{I, Z\}, \tau_\alpha \in \{I, X, Y, Z\}} c_\alpha \sigma_\alpha^{\otimes n-1} \otimes \tau_\alpha \quad (2)$$

where $\alpha \in \Lambda$, some index set and $c_\alpha \in \mathbb{R}$. In particular, the Hamiltonians corresponding to $\sigma_\alpha = Z, \tau_\alpha \in \{I, X, Y\}$ for all α are commonly used as local Hamiltonians in TFQIM Hamiltonians. These Hamiltonians are inspired by the structure of the Jordan-Wigner transformation of the Majorana fermion operators which are mapped as $Z^{\otimes n-1} \otimes X$ and $Z^{\otimes n-1} \otimes Y$, see [25], [2].

2. Quantum Ising Hamiltonian without any external field [46] is given by

$$\mathcal{H}_{\text{IM}} = \sum_{l=1}^{n-1} J_{l,l+1} Z_l Z_{l+1}, \quad (3)$$

where $J_{l,l+1} > 0$ denotes the interaction between adjacent sites $l, l+1$. Here we consider $J_{l,l+1} = J = 1 \forall l$. All the components of this standard Ising Hamiltonian in its expansion commutes, thus making it an excellent candidate for testing features of our circuit.

3. The Heisenberg Hamiltonian for both time-independent and dependent cases are commonly used in the study of magnetic systems in which magnetic spins are treated quantum mechanically [18], [57], [46]. Only spin-spin interactions are included in the said Hamiltonian with a random field, which is expressed as

$$\mathcal{H}_{\text{HEIS}} = \sum_{l=1}^{n-1} J_{l,l+1} (X_l X_{l+1} + Y_l Y_{l+1} + Z_l Z_{l+1}) + \sum_{l=1}^n h_l Z_l, \quad (4)$$

where $J_{l,l+1} > 0$ denotes the coupling parameter which specifies the exchange interaction between nearest-neighbour spin. We set $J_{l,l+1} = J$, a constant. Furthermore, we have taken $J = 1$, which depicts the antiferromagnetic case. Besides, h_l denotes the uniformly random coefficients which are chosen from a standard normal distribution on $[-1, 1]$.

The Hamiltonian can be further modified by invoking certain constraints such as interaction with the magnetic field that depends on time. In such cases the Hamiltonian becomes,

$$\mathcal{H}_{\text{HEIS}}(t) = \mathcal{H}_{\text{HEIS}} - g(t) \sum_{l=1}^N X_l, \quad (5)$$

where $g(t) = \sin \frac{\omega(t)\pi}{2}$ such that $\omega(t)$ takes the value 1 or -1 depending on even or odd time-steps respectively during unitary evolution.

4. Along with sparse Hamiltonians, we also investigate the transverse magnetic field quantum Ising model (TFQIM) with nearest-neighbor interactions defined as [46]

$$\mathcal{H}_{\text{TFQIM}} = J \sum_{l=1}^{n-1} Z_l Z_{l+1} + g \sum_{l=1}^n X_l + \sum_{l=1}^n h_l Z_l. \quad (6)$$

Here the sum runs over site l and l and $l+1$ denotes the nearest neighbour pair. $J > 0$ denotes the short-range interaction and g sets the transverse field strength which fosters spin alignment along the x -axis. For time-independent case, we shall consider J to be constant and equal to 1 and $g = \frac{J}{2}$. Here also the uniformly random coefficients h_l is chosen from a standard normal distribution on $[-1, 1]$.

Similarly, the Hamiltonian for time-dependent TFQIM takes the following form

$$\mathcal{H}_{\text{TFQIM}}(t) = J(t) \sum_{l=1}^{n-1} Z_l Z_{l+1} + g(t) \sum_{l=1}^n X_l + \sum_{l=1}^n h_l Z_l, \quad (7)$$

the value $J(t)$ oscillates between 1 and 0 depending on the even and odd time-steps and $g(t) = \frac{1}{2}$.

3.2 First-order Suzuki-Trotter expansion via quantum circuits

Hamiltonian simulation is performed by approximating the time-evolution unitary at each time step via a quantum circuit by employing a decomposition of the unitary such as Suzuki-Trotter decomposition scheme or Trotterization [22],[43]. In this paper we stick to the first-order Trotterization given by

$$U(T) = e^{-\iota HT} \approx \left(e^{-\iota HT/r} \right)^r \approx \left(\prod_{j=1}^L e^{-\iota a_j H_j T/r} \right)^r \quad (8)$$

for a time-independent Hamiltonian given by equation (1) with $O(T^2/R^2)$ approximation error for some positive integer r , known as the Trotter parameter and H is given by equation (1) [47]. Thus, to simulate the Hamiltonian over a long time T , the evolution is segmented into r Trotter steps, while preserving an error level of at most ϵ/r , where $\epsilon > 0$ such that the Trotter approximation error $\left\| U(T) - \left(\prod_{j=1}^L e^{-\iota a_j H_j T/r} \right)^r \right\|_F \leq \epsilon$. However, in practice, it is crucial to decide the value of the Trotter parameter r while performing the simulation. The first-order deterministic error is given by $r_{1, \text{det}} = O((T\lambda L)^2/\epsilon r^2)$, where $\lambda := \max_j \|H_j\|_2$, L is the total number of local Hamiltonian operators and ‘det’ indicates that these formulas are constructed deterministically [9] [7] [11]. Now, according to Equation 8, quantum circuits generate a succession of blocks responsible for performing specific time evolution, with their depth increasing linearly with r .

For time-dependent Hamiltonians i.e. when $a_j(t)$ is non-constant for some values of j in equation (1) then two approximations are employed to simulate the time evolution operator [62] [47]. It is first approximated as a piece-wise constant function by discretizing the time interval $[0, T]$ into small intervals of length Δt during which the time-dependent Hamiltonian remains constant, and in the second, during that time interval, the matrix exponential of the Hamiltonian is approximated using first-order Trotter decompositions as discussed above [62] [47]. Thus the time evolution operator is approximated as

$$U(T) \approx \prod_{k=1}^r \exp(-iH(k\Delta t)\Delta t) \quad (9)$$

where j multiplies over the number of discretized time-steps $\Delta t = T/r$, r is the number of time-steps of length Δt . The choice of r needs to ensure that Δt should be less than the fluctuation time-scale of $H(\Delta t)$ and the decomposition error is less than ϵ . Indeed, for time-dependent cases $a_j(t)$ is a piece-wise constant function i.e. $a_j(t) = a_j((m-1)\Delta t)$, $t \in [(m-1)\Delta t, m\Delta t]$, $m \in \{1, \dots, r\}$. In such cases $U(T) \approx \prod_{m=1}^r e^{-iH(m\Delta t)\Delta t} \approx \prod_{m=1}^r \prod_{j=1}^L e^{-ia_j(\Delta t)H_j\Delta t}$.

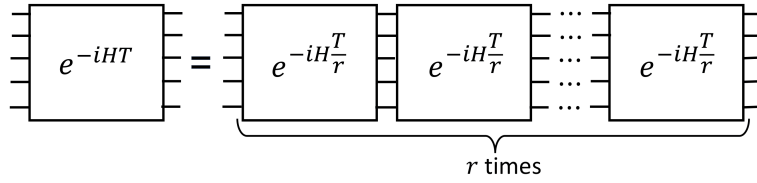


Figure 1: Trotter approximation through quantum circuit

Thus, simulating a Hamiltonian through quantum circuits boils down to efficient quantum circuit implementation of evolution of local Hamiltonian operators given by $\exp(-iH_j\theta)$, for some constant $\theta > 0$. Since the parametrized one-qubit gates and two-qubit control gates form a universal model of quantum computation, quantum circuits with optimal number of such gates for scalable implementation of exponential of scaled Pauli-strings, which are the local Hamiltonians in general, is the fundamental matter of concern here. Upon achieving this, the quantum circuit design employing equations (8) and (9), the probability distribution corresponding to the desired quantum state $|\psi(T)\rangle$ can be obtained for the input state $|\psi(0)\rangle$ after the quantum measurement of the output state of the quantum circuit with respect to computational basis.

The efficiency of quantum circuits is characterized by several circuit parameters for its implementation on a quantum hardware. For instance, quantum circuit depth is a measurement of the number of “layers” of quantum gates that must operate concurrently to complete the computation through the circuit [49]. Besides, the *qubit mapping problem* caused by limited two-qubit coupling on a low-connectivity hardware makes a quantum circuit not directly executable [33]. Finally, noisy implementation of quantum operations in physical quantum hardware adds another dimension for the analysis of different sources of noise for performing quantum circuit simulation [6]. In the next section, we briefly review some of the standard noise models considered for analyzing quantum circuit simulations.

3.3 Noise Model

Generally, the noise in a quantum circuit is considered of two types: per-gate noise and per-time noise [13]. In the first case, the noise is available at a constant rate per gate, independent of the time it takes to implement that gate which is a standard practice in quantum computation and the

model which we have implemented in this paper. In the second noise model, it is considered that noise occurs at a constant rate per unit time and is mainly used in developing error models in physics which we consider in this paper.

Now, it is to be noted that several techniques have been developed to analyze the state evolution of a quantum system in the presence of noise [53]. Among these, the Kraus operator formalism [29] stands out as one of the most prevalent methods. Under this formalism the evolution of a quantum state through a noisy quantum circuit is given by [42],

$$\rho' = \sum_j E_j \rho E_j^\dagger, \quad (10)$$

where $\rho = |\psi\rangle\langle\psi|$ i.e. the density matrix; as we are only dealing with pure quantum state $|\psi\rangle$ and the E_j represent Kraus operators associated with various noise channels, satisfying the condition $\sum_j E_j E_j^\dagger = I$, where I denotes the identity operator [42]. The density matrices ρ' and ρ correspond to the states after and before undergoing a noisy quantum channel, respectively. In our study, we restrict ourselves to four noisy quantum channels described below, where p is error probability such that $0 \leq p \leq 1$.

1. Gate error: The Kraus operators corresponding to the bit-flip channel are $E_0 = \sqrt{1-p}I_2$, $E_1 = \sqrt{p}X$, and for the phase-flip channel $E_0 = \sqrt{1-p}I_2$, $E_1 = \sqrt{p}Z$.
2. Idle error: The Kraus operators corresponding to the amplitude-damping channel are $E_0 = \begin{pmatrix} 1 & 0 \\ 0 & \sqrt{1-p} \end{pmatrix}$, $E_1 = \begin{pmatrix} 1 & \sqrt{p} \\ 0 & 0 \end{pmatrix}$, and for the Phase damping channel $E_0 = \begin{pmatrix} 1 & 0 \\ 0 & \sqrt{1-p} \end{pmatrix}$, $E_1 = \begin{pmatrix} 1 & 0 \\ 0 & \sqrt{p} \end{pmatrix}$.

We incorporate these error models in the proposed quantum circuit simulation with varying degrees of error in order to observe their impact on the circuit and in turn, simulation of the Hamiltonian, see Section 6.

4 Circuit model for Pauli string exponential

In this section, we develop scalable quantum circuit for exponential of scaled Pauli-strings. As a result, we lay the ground work for Hamiltonian simulation via circuit model of computation.

First, we introduce the following notations. For a given $x \in \{0, \dots, 2^{n-1} - 1\}$ with its binary representation (x_{n-2}, \dots, x_0) such that $x = \sum_{j=0}^{n-2} x_j 2^j$, $x_j \in \{0, 1\}$, we define a circuit in the following way. For each x_j , $0 \leq j \leq n-2$ the circuit contains a $\text{CNOT}_{(n,n-j-1)}$ gate if the $x_j = 1$, where $\text{CNOT}_{(n,n-j-1)}$ denotes a CNOT gate with n -th qubit as the control and $(n-j-1)$ -th qubit as target. Since any CNOT gate represents a permutation matrix, we define new permutations as product of CNOT gates as follows, which we play a primary role in the sequel. We denote these permutations as

$$\begin{aligned} \Pi_{n,x}^e &= \prod_{j=0}^{n-2} \delta_{1,x_j} \text{CNOT}_{(n,n-j-1)} \\ \Pi_{n,x}^o &= (\text{CNOT}_{(n-m-1,n)})(\Pi_{n,x}^e)(\text{CNOT}_{(n-m-1,n)}) \end{aligned} \quad (11)$$

where m is the greatest integer $0 \leq m \leq n-2$ such that $x_m = 1$ in the binary string of $x = (x_{n-2} \dots x_0)$ i.e. $m = \max\{j | \delta_{1,x_j} = 1\}$ and δ denotes Kronecker delta function. For $x = 0$, we consider $\Pi\Gamma_{n,x}^e$ and $\Pi\Gamma_{n,x}^o$ as the identity matrix i.e. absence of any CNOT gates.

Then we recall some permutation matrices associated with CNOT gates from [54] [55]. The set of binary strings $\{(x_{n-2}, x_2, \dots, x_0) : x_j \in \{0, 1\}\}$ and the set of all subsets of $[n-1] := \{1, \dots, n-1\}$ have a one-one correspondence defined by $\chi : \{0, 1\}^{n-1} \rightarrow 2^{[n-1]}$, which assigns $x = (x_{n-2}, x_{n-3}, \dots, x_0)$ to $\chi(x) = \Lambda_x := \{j : x_j = 1, 1 \leq j \leq n-1\} \subseteq [n-1]$. Thus each position of the string represents a characteristic function for Λ_x . Then we rewrite the following theorem from [55].

Theorem 4.1. *Let $\chi : \{0, 1\}^{n-1} \rightarrow 2^{[n-1]}$ be the bijective function as defined above such that $\chi(x) = \Lambda_x$. For any $x \equiv (x_{n-2}, \dots, x_0) \in \{0, 1\}^{n-1}$, define the functions $\alpha_{\Lambda_x}^g : \{0, 1\}^{n-1} \rightarrow \{0, \dots, 2^{n-1} - 1\}$ and $\beta_{\Lambda_x}^g : \{0, 1\}^{n-1} \rightarrow \{0, \dots, 2^{n-1} - 1\}$, $g \in \{e, o\}$ as*

$$\begin{aligned} \alpha_{\Lambda_x}^g(m) &= \sum_{k \in \Lambda_x} m_k 2^{k+1} + \sum_{j \notin \Lambda_x} m_j 2^{j+1} + 2, \quad \beta_{\Lambda_x}^e(m) = \sum_{k \in \Lambda_x} \bar{m}_k 2^{k+1} + \sum_{j \notin \Lambda_x} m_j 2^{j+1} + 2, \\ \beta_{\Lambda_x}^o(m) &= \sum_{k \in \Lambda_x} \bar{m}_k 2^{k+1} + \sum_{j \notin \Lambda_x} m_j 2^{j+1} + 1, \end{aligned}$$

with $m = (m_{n-2}, \dots, m_0)$ and $\bar{m}_k = m_k \oplus 1$. Then

$$\Pi\Gamma_{n,x}^g = \prod_{m=0, \alpha_{\Lambda_x}^g(m) < \beta_{\Lambda_x}^g(m)}^{2^{n-1}-1} P_{(\alpha_{\Lambda_x}^g(m), \beta_{\Lambda_x}^g(m))}, \quad g \in \{e, o\}.$$

Further $\Pi\Gamma_{n,x}^g \neq \Pi\Gamma_{n,y}^g$ if $x \neq y$ and $(\alpha_{\Lambda_x}^g(m), \beta_{\Lambda_x}^g(m)) \neq (\alpha_{\Lambda_y}^g(m), \beta_{\Lambda_y}^g(m))$ for all $0 \leq m \leq 2^{n-1} - 1$.

4.1 Permutation-similarity of Pauli-strings

In this section, we provide a circuit model to establish a similarity relation between Pauli-strings containing X gate and I_2 through permutation matrices defined above. First we introduce the following notations.

For any integer $b \in \{0, \dots, 2^n - 1\}$ consider the binary representation of b as (b_1, \dots, b_n) , $b_j \in \{0, 1\}$ such that $b = \sum_{j=1}^n 2^{n-j} b_j$. Then corresponding to any such b , define the Pauli-string matrix $\sigma_b = \otimes_{j=1}^n \sigma_j = \sigma_1 \otimes \dots \otimes \sigma_n$, where

$$\sigma_j = \begin{cases} X & \text{if } b_j = 1 \\ I_2 & \text{if } b_j = 0. \end{cases}$$

This notation enables to define an ordering on the set $S_{I_2, X}^{(n)} = \{\sigma_b | 0 \leq b \leq 2^n - 1\}$ based on the standard ordering of the set $\{0, \dots, 2^n - 1\}$ defined by the map $\eta_n : S_{I_2, X}^{(n)} \rightarrow \{0, 1, \dots, 2^n - 1\}$ as $\eta_n(\sigma_b) = b$. Besides, the canonical basis of the n -qubit Hilbert space can be written as $\{|b\rangle : 0 \leq b \leq 2^n - 1\} = \{|b_1 \dots b_n\rangle | b_j \in \{0, 1\}\}$.

Now we have the following theorem, which establishes permutation similarity of Pauli-strings defined by Pauli matrices I_2, X .

Theorem 4.2. *Let $b \in \{1, \dots, 2^n - 1\}$. Then*

$$\sigma_b = \begin{cases} \Pi\Gamma_{n, \frac{b-1}{2}}^e (I_2^{\otimes(n-1)} \otimes X) \Pi\Gamma_{n, \frac{b-1}{2}}^e, & \text{if } b \text{ is odd} \\ \Pi\Gamma_{n, \frac{b}{2}}^o (I_2^{\otimes(n-1)} \otimes X) \Pi\Gamma_{n, \frac{b}{2}}^o, & \text{if } b \text{ is even.} \end{cases}$$

Proof: Let $|\psi\rangle = |\psi_1 \dots \psi_n\rangle$, $|\psi_j\rangle = a_j |0\rangle + b_j |1\rangle$ be an n -qubit input quantum state for unitary matrix represented by the product of sequence of quantum gates given by $\Pi\Gamma_{n,x}^g(I_2^{\otimes(n-1)} \otimes X)\Pi\Gamma_{n,x}^g$. Then we need to show that the output becomes $\sigma_b |\psi\rangle$ for some $b = (b_1 \dots b_n) \in \{0,1\}^n$ and $\sigma_b = \sigma_1 \otimes \dots \otimes \sigma_n$ with $\sigma_j = X$ if $b_k = 1$ and $\sigma_k = I_2$ if $b_k = 0$.

Let $x \in \{0,1,\dots,2^{n-1}-1\}$ with the binary representation $x \equiv (x_{n-2}, \dots, x_0) \in \{0,1\}^{n-1}$. Suppose $J = \{j_1, \dots, j_l\} \subseteq \{0, \dots, n-2\}$ such that $x_j = 1$ if $j \in J$ and $x_j = 0$ if $j \notin J$. Further, let $j_1 < j_2 < \dots < j_l$. Now first consider $g = e$. Then

$$\begin{aligned}
& \Pi\Gamma_{n,x}^e(I_2^{\otimes n-1} \otimes X)\Pi\Gamma_{n,x}^e |\psi\rangle \\
&= \Pi\Gamma_{n,x}^e(I_2^{\otimes n-1} \otimes X)\Pi\Gamma_{n,x}^e(a_n |\psi_1 \dots \psi_{n-1}0\rangle + b_n |\psi_1 \dots \psi_{n-1}1\rangle) \\
&= \Pi\Gamma_{n,x}^e(I_2^{\otimes n-1} \otimes X)(a_n |\psi_1 \dots \psi_{n-1}0\rangle + b_n |\psi_1 \dots (X\psi_{n-j_l-1}) \dots (X\psi_{n-j_1-1}) \dots 1\rangle) \\
&= \Pi\Gamma_{n,x}^e(a_n |\psi_1 \dots \psi_{n-1}1\rangle + b_n |\psi_1 \dots (X\psi_{n-j_l-1}) \dots (X\psi_{n-j_1-1}) \dots 0\rangle) \\
&= a_n |\psi_1 \dots (X\psi_{n-j_l-1}) \dots (X\psi_{n-j_1-1}) \dots 1\rangle + b_n |\psi_{n-1} \dots (X\psi_{n-j_l-1}) \dots (X\psi_{n-j_1-1}) \dots 0\rangle \\
&= |\psi_1 \dots (X\psi_{n-j_l-1}) \dots (X\psi_{n-j_1-1}) \dots (X\psi_n)\rangle \\
&= \sigma_b |\psi\rangle,
\end{aligned}$$

where $\sigma_b = \sigma_1 \otimes \dots \otimes \sigma_n$ such that $\sigma_{n-j-1} = X$ if $j \in J$ and I_2 otherwise and also $\sigma_n = X$. From our definition $x = \sum_{j \in J} 2^j$ and $b = \sum_{j \in J} 2^{n-(n-j-1)} + 1 = \sum_{j \in J} 2^{j+1} + 1$ is odd and thus $x = \frac{b-1}{2}$. Now taking $g = o$,

$$\begin{aligned}
& \Pi\Gamma_{n,x}^o(I_2^{\otimes n-1} \otimes X)\Pi\Gamma_{n,x}^o |\psi\rangle \\
&= (\text{CNOT})_{(n-j_l-1,n)}\Pi\Gamma_{n,x}^e(\text{CNOT})_{(n-j_l-1,n)}(I_2^{\otimes n-1} \otimes X)(\text{CNOT})_{(n-j_l-1,n)}\Pi\Gamma_{n,x}^e(\text{CNOT})_{(n-j_l-1,n)} |\psi\rangle \\
&= (\text{CNOT})_{(n-j_l-1,n)}\Pi\Gamma_{n,x}^e(\text{CNOT})_{(n-j_l-1,n)}(I_2^{\otimes n-1} \otimes X)(\text{CNOT})_{(n-j_l-1,n)}\Pi\Gamma_{n,x}^e(\text{CNOT})_{(n-j_l-1,n)} \\
&\quad (a_{n-j_l-1} |\psi_1 \dots \psi_{n-j_l-2}0\psi_{n-j_l} \dots \psi_n\rangle + b_{n-j_l-1} |\psi_1 \dots \psi_{n-j_l-2}1\psi_{n-j_l} \dots \psi_n\rangle) \\
&= (\text{CNOT})_{(n-j_l-1,n)}\Pi\Gamma_{n,x}^e(\text{CNOT})_{(n-j_l-1,n)}(I_2^{\otimes n-1} \otimes X)(\text{CNOT})_{(n-j_l-1,n)}\Pi\Gamma_{n,x}^e \\
&\quad (a_{n-j_l-1} |\psi_1 \dots \psi_{n-j_l-2}0\psi_{n-j_l} \dots \psi_n\rangle + b_{n-j_l-1} |\psi_1 \dots \psi_{n-j_l-2}1\psi_{n-j_l} \dots (X\psi_n)\rangle) \\
&= (\text{CNOT})_{(n-j_l-1,n)}\Pi\Gamma_{n,x}^e(\text{CNOT})_{(n-j_l-1,n)}(I_2^{\otimes n-1} \otimes X)(\text{CNOT})_{(n-j_l-1,n)}\Pi\Gamma_{n,x}^e \\
&\quad (a_{n-j_l-1}a_n |\psi_1 \dots \psi_{n-j_l-2}0\psi_{n-j_l} \dots 0\rangle + a_{n-j_l-1}b_n |\psi_1 \dots \psi_{n-j_l-2}0\psi_{n-j_l} \dots 1\rangle \\
&\quad + b_{n-j_l-1}a_n |\psi_1 \dots \psi_{n-j_l-2}1\psi_{n-j_l} \dots 0\rangle + b_{n-j_l-1}b_n |\psi_1 \dots \psi_{n-j_l-2}1\psi_{n-j_l} \dots 1\rangle) \\
&= (\text{CNOT})_{(n-j_l-1,n)}\Pi\Gamma_{n,x}^e(\text{CNOT})_{(n-j_l-1,n)}(I_2^{\otimes n-1} \otimes X)(\text{CNOT})_{(n-j_l-1,n)} \\
&\quad (a_{n-j_l-1}a_n |\psi_1 \dots \psi_{n-j_l-2}0\psi_{n-j_l} \dots 0\rangle + a_{n-j_l-1}b_n |\psi_1 \dots \psi_{n-j_l-2}1\psi_{n-j_l} \dots (X\psi_{n-j_1-1}) \dots 1\rangle \\
&\quad + b_{n-j_l-1}a_n |\psi_1 \dots \psi_{n-j_l-2}1\psi_{n-j_l} \dots 0\rangle + b_{n-j_l-1}b_n |\psi_1 \dots \psi_{n-j_l-2}0\psi_{n-j_l} \dots (X\psi_{n-j_1-1}) \dots 1\rangle)
\end{aligned}$$

$$\begin{aligned}
&= (\text{CNOT})_{(n-j_l-1,n)} \Pi \Gamma_{n,x}^e (\text{CNOT})_{(n-j_l-1,n)} (I_2^{\otimes n-1} \otimes X) \\
&\quad (a_{n-j_l-1} a_n |\psi_1 \dots \psi_{n-j_l-2} 0 \psi_{n-j_l} \dots 0\rangle + a_{n-j_l-1} b_n |\psi_1 \dots \psi_{n-j_l-2} 1 \psi_{n-j_l} \dots (X \psi_{n-j_l-1}) \dots 0\rangle \\
&\quad + b_{n-j_l-1} a_n |\psi_1 \dots \psi_{n-j_l-2} 1 \psi_{n-j_l} \dots 1\rangle + b_{n-j_l-1} b_n |\psi_1 \dots \psi_{n-j_l-2} 0 \psi_{n-j_l} \dots (X \psi_{n-j_l-1}) \dots 1\rangle) \\
&= (\text{CNOT})_{(n-j_l-1,n)} \Pi \Gamma_{n,x}^e (\text{CNOT})_{(n-j_l-1,n)} \\
&\quad (a_{n-j_l-1} a_n |\psi_1 \dots \psi_{n-j_l-2} 0 \psi_{n-j_l} \dots 1\rangle + a_{n-j_l-1} b_n |\psi_1 \dots \psi_{n-j_l-2} 1 \psi_{n-j_l} \dots (X \psi_{n-j_l-1}) \dots 1\rangle \\
&\quad + b_{n-j_l-1} a_n |\psi_1 \dots \psi_{n-j_l-2} 1 \psi_{n-j_l} \dots 0\rangle + b_{n-j_l-1} b_n |\psi_1 \dots \psi_{n-j_l-2} 0 \psi_{n-j_l} \dots (X \psi_{n-j_l-1}) \dots 0\rangle) \\
&= (\text{CNOT})_{(n-j_l-1,n)} \Pi \Gamma_{n,x}^e \\
&\quad (a_{n-j_l-1} a_n |\psi_1 \dots \psi_{n-j_l-2} 0 \psi_{n-j_l} \dots 1\rangle + a_{n-j_l-1} b_n |\psi_1 \dots \psi_{n-j_l-2} 1 \psi_{n-j_l} \dots (X \psi_{n-j_l-1}) \dots 0\rangle \\
&\quad + b_{n-j_l-1} a_n |\psi_1 \dots \psi_{n-j_l-2} 1 \psi_{n-j_l} \dots 1\rangle + b_{n-j_l-1} b_n |\psi_1 \dots \psi_{n-j_l-2} 0 \psi_{n-j_l} \dots (X \psi_{n-j_l-1}) \dots 0\rangle) \\
&= (\text{CNOT})_{(n-j_l-1,n)} (a_{n-j_l-1} a_n |\psi_1 \dots \psi_{n-j_l-2} 1 \psi_{n-j_l} \dots (X \psi_{n-j_l-1}) \dots 1\rangle \\
&\quad + a_{n-j_l-1} b_n |\psi_1 \dots \psi_{n-j_l-2} 1 \psi_{n-j_l} \dots (X \psi_{n-j_l-1}) \dots 0\rangle \\
&\quad + b_{n-j_l-1} a_n |\psi_1 \dots \psi_{n-j_l-2} 0 \psi_{n-j_l} \dots (X \psi_{n-j_l-1}) \dots 1\rangle \\
&\quad + b_{n-j_l-1} b_n |\psi_1 \dots \psi_{n-j_l-2} 0 \psi_{n-j_l} \dots (X \psi_{n-j_l-1}) \dots 0\rangle) \\
&= (a_{n-j_l-1} a_n |\psi_1 \dots \psi_{n-j_l-2} 1 \psi_{n-j_l} \dots (X \psi_{n-j_l-1}) \dots 0\rangle \\
&\quad + a_{n-j_l-1} b_n |\psi_1 \dots \psi_{n-j_l-2} 1 \psi_{n-j_l} \dots (X \psi_{n-j_l-1}) \dots 1\rangle \\
&\quad + b_{n-j_l-1} a_n |\psi_1 \dots \psi_{n-j_l-2} 0 \psi_{n-j_l} \dots (X \psi_{n-j_l-1}) \dots 1\rangle \\
&\quad + b_{n-j_l-1} b_n |\psi_1 \dots \psi_{n-j_l-2} 0 \psi_{n-j_l} \dots (X \psi_{n-j_l-1}) \dots 0\rangle) \\
&= |\psi_1 \dots (X \psi_{n-j_l-1}) \dots (X \psi_{n-j_l-1}) \dots \psi_n\rangle = \sigma_b |\psi\rangle,
\end{aligned}$$

where $\sigma_b = \sigma_1 \otimes \dots \otimes \sigma_n$ such that $\sigma_{n-j-1} = X$ if $j \in J$ and I_2 otherwise. From our definition $x = \sum_{j \in J} 2^j$ and $b = \sum_{j \in J} 2^{n-(n-j-1)} = \sum_{j \in J} 2^{j+1}$ is even and thus $x = \frac{b}{2}$. When $x = 0$, the case is trivial and this completes the proof. \square

Remark 4.3. Note that

$$\begin{aligned}
&|\{\Pi \Gamma_{n,x}^e : 1 \leq x \leq 2^{n-1} - 1\} \cup \{\Pi \Gamma_{n,x}^o : 1 \leq x \leq 2^{n-1} - 1\} \cup I_{2^n}| \\
&= |\{\Pi \Gamma_{n,x}^e : 1 \leq x \leq 2^{n-1} - 1\}| + |\{\Pi \Gamma_{n,x}^o : 1 \leq x \leq 2^{n-1} - 1\}| + 1 \\
&= 2^n - 1
\end{aligned}$$

This is due to the fact that $\{\Pi \Gamma_{n,x}^e : 1 \leq x \leq 2^{n-1} - 1\} \cap \{\Pi \Gamma_{n,x}^o : 1 \leq x \leq 2^{n-1} - 1\} = \emptyset$. Further, from [54], it is to be noticed that all permutations from $\{\Pi \Gamma_{n,x}^e : 1 \leq x \leq 2^{n-1} - 1\} \cup \{\Pi \Gamma_{n,x}^o : 1 \leq x \leq 2^{n-1} - 1\} \cup I_{2^n}$ are distinct even in their components i.e. no two components of the transpositions match because each permutation matrix has unique circuit construction. Also $|\mathcal{S}_{I,X}^{(n)} \setminus \{I\}| = 2^n - 1$. Hence, there is a 1-1 correspondence between $\{\Pi \Gamma_{n,x}^e : 1 \leq x \leq 2^{n-1} - 1\} \cup \{\Pi \Gamma_{n,x}^o : 1 \leq x \leq 2^{n-1} - 1\} \cup I_{2^n}$ and $\mathcal{S}_{I,X}^{(n)} \setminus \{I\}$ through the operation $\Pi \Gamma_{n,x}^g (I_2^{\otimes n-1} \otimes X) \Pi \Gamma_{n,x}^g, g \in \{e, o\}$. \square

We also recall that $HXH = Z$ and $Y = S^\dagger X S$ where

$$H = \frac{1}{\sqrt{2}} \begin{bmatrix} 1 & 1 \\ 1 & -1 \end{bmatrix}, \text{ and } S = \begin{bmatrix} e^{i\pi/4} & 0 \\ 0 & e^{-i\pi/4} \end{bmatrix} = R_Z(\pi/4),$$

\dagger denotes conjugate transpose of a matrix and $R_Z(\theta) = \begin{bmatrix} \exp(i\theta) & 0 \\ 0 & \exp(-i\theta) \end{bmatrix}$ denotes the rotation gate of a qubit around Z -axis by an angle θ . Then we have the following theorem.

Theorem 4.4. For any n -length Pauli string $\sigma_1 \otimes \sigma_2 \dots \otimes \sigma_n$, $\sigma_j \in \{I, X, Y, Z\}$ the following relation holds

$$(\sigma_1 \otimes \sigma_2 \dots \otimes \sigma_n) = (\tau_1 \otimes \tau_2 \dots \otimes \tau_n)^\dagger (\mu_1 \otimes \mu_2 \dots \otimes \mu_n) (\tau_1 \otimes \tau_2 \dots \otimes \tau_n)$$

where

$$\begin{cases} \tau_j = H, \mu_j = X, & \text{if } \sigma_j = Z \\ \tau_j = S, \mu_j = X, & \text{if } \sigma_j = Y \\ \tau_j = I, \mu_j = X, & \text{if } \sigma_j = X \\ \tau_j = I, \mu_j = I, & \text{if } \sigma_j = I, \end{cases}$$

$$j \in \{0, \dots, n-1\}.$$

Proof: Follows from elementary application of Kronecker product and $HXH = Z$ and $Y = S^\dagger XS$. \square

4.2 Design of scalable quantum circuits for exponential of Pauli-strings

In this section, we shall provide a scalable quantum circuit model representation of Pauli-string exponentials using only 1-qubit rotation gates and CNOT gates.

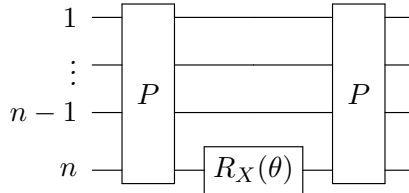
It is obvious to see that circuit for $\exp(i\theta I_2^{\otimes(n-1)} \otimes X)$ is

$$\begin{array}{c} 1 \text{ --- } \\ 2 \text{ --- } \\ \vdots \text{ --- } \\ n \text{ --- } \boxed{R_X(\theta)} \text{ --- } \end{array} \quad (12)$$

where $R_X(\theta) = \begin{bmatrix} \cos \theta & i \sin \theta \\ i \sin \theta & \cos \theta \end{bmatrix}$ denotes the qubit's rotation gate around the X -axis by an angle of θ .

Now, we have the following Theorem.

Theorem 4.5. Given any n -length Pauli string $\sigma \in \mathcal{S}_{I,X}^{(n)} \setminus \{I_{2^n}\}$. Then the circuit for $\exp(i\theta\sigma)$ is given as

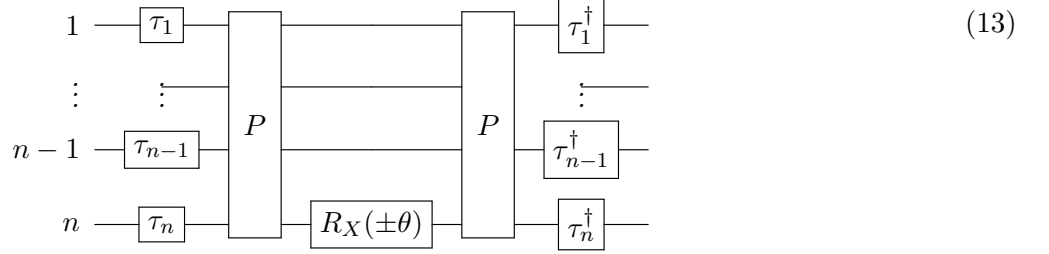


where $P \in \{\Pi \Gamma_{n,x}^g : g \in \{e, o\}, 0 \leq x \leq 2^{n-1} - 1\}$ is a permutation matrix mentioned Theorem 4.2 such that $P\sigma P = I_2^{\otimes(n-1)} \otimes X$.

Proof: From Theorem 4.2, we see that any Pauli string $\sigma \in \mathcal{S}_{I,X}^{(n)} \setminus \{I\}$ can be written as $P\sigma P$ for some symmetric permutation matrix P where $\sigma^{(n)} = I_2^{\otimes(n-1)} \otimes X$. Clearly, from standard linear algebra, $\exp(i\theta\sigma) = P \exp(i\theta\sigma^{(n)}) P$. The rest of the proof follows immediately. \square

Finally, we show how to express exponential of any scaled n -length Pauli-string in a quantum circuit.

Corollary 4.6. *Given any n -length Pauli string such that $\sigma = (\sigma_1 \otimes \sigma_2 \dots \otimes \sigma_n) \neq I$. Then σ can be written in the form $(\sigma_1 \otimes \sigma_2 \dots \otimes \sigma_n) = (\tau_1 \otimes \tau_2 \dots \otimes \tau_n)^\dagger (\mu_1 \otimes \mu_2 \dots \otimes \mu_n) (\tau_1 \otimes \tau_2 \dots \otimes \tau_n)$ where $\tau_j, \mu_j, j \in \{1, \dots, n\}$ are Pauli matrices satisfying the conditions in Theorem 4.4. Then the circuit for $\exp(\pm i\theta\sigma)$ is given as*



where P is a permutation matrix derived from Theorem 4.2 such that $P(\mu_1 \otimes \mu_2 \dots \otimes \mu_n)P = I_2^{\otimes(n-1)} \otimes X$.

Proof: The proof follows from Theorem 4.4 and Theorem 4.5. Indeed, note that $\sigma = \tau\mu\tau$ implies $\exp(\pm i\theta\sigma) = \tau \exp(\pm i\theta\mu) \tau$ since $\tau = \bigotimes_{j=1}^n \tau_j$ is unitary and $\mu = \bigotimes_{j=1}^n \mu_j$. \square

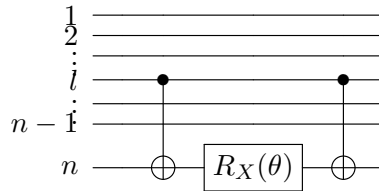
Now we provide Algorithm 1 for the construction of exponential of n -length Pauli-strings as discussed in the theorems above.

Hence, we formulate Algorithm 1 that helps us to convert any Pauli string in $S_n \setminus I_2^n$ to $I^{\otimes(n-1)} \otimes X$. Using Algorithm 1, it follows that deriving the matrix representation of elements of $\mathcal{S}_{I,X}^{(n)}$ can be performed in $O(2^{n-1})$.

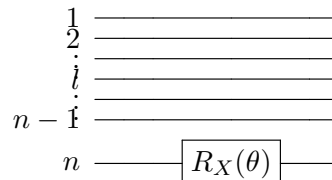
From the circuit of Pauli string exponentials, we prove the following theorem that showcases total number of CNOT and one-qubit rotation gates required for the circuit model.

Theorem 4.7. *Let σ be a n -length Pauli-string and let there be n_1, n_2, n_3 and n_4 number of X, Y, Z and I_2 gates respectively that comprise σ and $n = n_1 + n_2 + n_3 + n_4$. Then, the quantum circuit of $\exp(i\theta\sigma)$ requires at most 1 R_X gate, $2n_2$ R_Y gates, $4n_2 + 2n_3$ R_Z gates, $2n - 2$ gates of the form $\text{CNOT}_{n,l}$ and at most 2 gates of the form $\text{CNOT}_{l,n}$ where $l \in \{1, \dots, n-1\}$. If $\sigma \in \mathcal{S}_{I,Z}^{(n)}$, then at most $2n - 2$ gates of the form $\text{CNOT}_{l,n}$ and 1 R_Z gates are required to construct $\exp(i\theta\sigma)$.*

Proof: From the construction of exponential of Pauli strings in Algorithm 1 and Corollary 4.6, we see that all permutation matrices $\Pi \Gamma_{n,x}^g, 1 \leq x \leq 2^{n-1} - 1, g \in \{e, o\}$ require at most $n + 1$ CNOT gates. Such a bound is obtained for $\Pi \Gamma_{n,2^{n-1}-1}^o$, where $n - 1$ $\text{CNOT}_{l,n}$ gates and 2 $\text{CNOT}_{1,n}$ are required (See Theorem 4.1 or [54]). Since such permutation matrices are multiplied on both sides of $I^{\otimes(n-1)} \otimes X$, then at most $2n - 2$ $\text{CNOT}_{n,l}$ and 4 $\text{CNOT}_{l,n}$ gates are required. Now it is easy to see that the circuit



and



are equivalent.

Hence, at most $2 \text{ CNOT}_{l,n}$ are sufficient where $l \in \{1, \dots, n-1\}$. Further from Corollary 4.6, and Algorithm 1 each $\tau_j, 0 \leq j \leq n-1$ require $2 R_Z$ gates and $1 R_Y$ gates when $\tau_j = H$. When $\tau_j = S = R_Z(\pi/4)$, only one R_Z is needed. Such single-qubit gates are multiplied both sides i.e. added to both ends of the quantum circuit. Hence, the result follows. \square

As mentioned in Section 3.2, there are several approaches proposed in the literature to design and implement exponential of scaled Pauli-strings through quantum circuits. These methods along with the method proposed in this paper can be compared dealing with three properties of the circuits: scalability, partition methods for Pauli-strings using a linear algebraic such as simultaneous diagonalization [63] or an optimization technique, using a specific gate such as T gate in the synthesis that is hard to implement in a quantum hardware [20], and the assumption of fully connected qubits in the quantum hardware. It follows from the proposed quantum circuit design in this paper that it does not need any partitioning method to determine commutative Pauli-strings, and it is scalable with CNOT and one-qubit gates. Besides, the circuit bypasses the need of complete connectivity owing to the construction of permutation matrices where the circuit only requires all qubits to have connectivity with the n -th qubit which shows potential to be compatible with near term quantum computer architecture for certain number of qubits such as IBM Q5 Yorktown/IBM QX2 quantum architecture for 5 qubits [14]. We display a comparison of the available techniques in the literature in Table 2.

Ref.	Scalability	Partitioning	Gate set	Full connectivity of Hardware required
[50]	No	Yes	Clifford+T	Yes (NE)
[63]	No	Yes	Clifford+T	No
[41]	No	Yes	Clifford+T	Yes (NE)
[24]	No	Yes	Clifford+T	NE
[67]	No	Yes	CNOT+one-qubit	Yes
[38]	Yes (NE)	No	CNOT+one-qubit	Yes
[13]	No	Yes	CNOT+one-qubit	No
[51]	No	Yes	CNOT+one-qubit	Yes (NE)
This paper	Yes	No	CNOT+one-qubit	No

Table 2: Comparison for quantum circuit synthesis of Pauli-string exponential with available method in literature. The abbreviation NE stands for “Not Emphasized” in the paper.

Algorithm 1 Constructing circuits of any n -length Pauli string exponentials

Provided:

1. n -length Pauli strings that is not $I^{\otimes n}$
2. $\{\Pi T_{n,x}^e | 1 \leq x \leq 2^{n-1} - 1\}, \{\Pi T_{n,x}^o | 1 \leq x \leq 2^{n-1} - 1\}$ as defined in equation 11 and Theorem 4.1
3. Hadamard gate H and $S = R_Z(\pi/4)$

Input: A n -length Pauli string $\sigma = \sigma_1 \otimes \dots \otimes \sigma_n \neq I^{\otimes n}$ where $\sigma_j \in \{I, X, Y, Z\}, j \in \{1, \dots, n\}$.

Output: Quantum circuit for $\exp(\pm i\theta\sigma)$

```
J → ∅
J1 → ∅
J2 → ∅
for k = 1 : n : k++ do
    μk → I
    τk → I
End For
for k = 1 : n : k++ do
    if σk == X then
        J → J ∪ {k}
    else if σk == Y then
        J1 → J1 ∪ {k}
    else if σk == Z then
        J2 → J2 ∪ {k}
    End If
End For
for k = 1 : n : k++ do
    if k ∈ J and k ∈ J1 then
        μk → X
    End If
End For
μ → μ1 ⊗ ... ⊗ μn
b → ∑k ∈ J ∪ J1n 2n-k
if b is odd then
    x →  $\frac{b-1}{2}$ 
    P → ΠTx,ne
else
    x →  $\frac{b}{2}$ 
    P → ΠTx,no
End If
for k = 1 : n : k++ do
    if k ∈ J1 then
        τk → S
    else if σk == Z then
        τk → H
    End If
End For
```

Output: Circuit 13

End

5 Hamiltonian simulation via quantum circuits

In this section, we report the empirical error of approximating $U(t)$ using first-order Suzuki-Trotter formula and simulating the quantum circuits corresponding to scaled Pauli-strings as discussed in Section 4 for both time-independent and time-dependent Hamiltonian operators described in Section 3.1. Indeed, we show that circuit simulation error matches with the numerical Trotter approximation error. We also identify a salient feature of the proposed quantum circuit model in simulating certain Hamiltonian operators that the proposed circuits have constant depth, see Section 5.1.1. Finally, we incorporate the noise models as described in Section 3.3 in order to investigate the efficiency of the proposed circuit model for Hamiltonian simulation in a NISQ like environment. All simulations have been carried out on Qiskit [48] on a system with 16GB RAM, 12th Gen Intel(R) Core(TM) i5-1235U; 1.30 GHz till 8-qubit examples. Beyond 8-qubit examples, we have performed the simulations using the supercomputer PARAM Shakti of IIT Kharagpur, established under National Supercomputing Mission (NSM), Government of India and supported by Centre for Development of Advanced Computing (CDAC), Pune [15].

5.1 Circuits for unitary evolution of local Hamiltonian operators

First we discuss the local Hamiltonian for the Hamiltonian operators considered in this paper and then we provide the specific quantum circuits associated with it.

- (a) $\mathcal{H}_{\text{BLKDG}}$: The local Hamiltonian operators are $I^{\otimes(n-1)} \otimes \sigma, Z^{\otimes(n-1)} \otimes \sigma, 0 \leq l \leq n-1$. Here $\sigma \in \{X, Z\}$, and as before, it represents a diagonal matrix when $\sigma = Z$.
- (b) \mathcal{H}_{IM} : The local Hamiltonian operators are $I^{\otimes l} \otimes Z \otimes Z \otimes I^{\otimes n-l-2}, 0 \leq l \leq n-2$.
- (c) $\mathcal{H}_{\text{HEIS}}$: The local-Hamiltonian operators are Pauli-strings given by
 1. $I^{\otimes l} \otimes \sigma \otimes \sigma \otimes I^{\otimes n-2-l}, 0 \leq l \leq n-2$
 2. $I^{\otimes l} \otimes \sigma \otimes I^{\otimes n-1-l}, 0 \leq l \leq n-1$

where $\sigma \in \{X, Y, Z\}$. Note that, when $\sigma = Z$ then the local Hamiltonian represents a diagonal matrix.

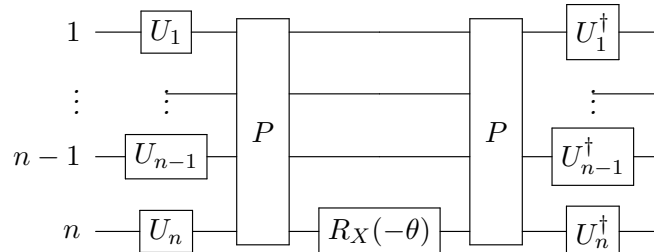
- (d) $\mathcal{H}_{\text{TFQIM}}$: The local Hamiltonian operators are Pauli-strings $I^{\otimes l} \otimes \sigma \otimes I^{\otimes n-1-l}, 0 \leq l \leq n-1$. Here $\sigma \in \{X, Z\}$, and as before, it represents a diagonal matrix when $\sigma = Z$.

The quantum circuits for evolution corresponding to these local Hamiltonian operators are described below following Section 4.

Theorem 5.1. *The quantum circuits for $\exp(-i\theta H)$,*

$$H \in \left\{ H_1 := \tau^{\otimes l} \otimes \sigma \otimes \tau^{\otimes n-1-l}, H_2 := \tau^{\otimes l} \otimes \sigma \otimes \sigma \otimes \tau^{\otimes n-2-l}, H_3 := \tau^{\otimes(n-1)} \otimes \sigma \right\},$$

$0 \leq l \leq n-1, \sigma \in \{X, Y\}$, and $\tau \in \{I, Z\}$ are given by



where

$$P = \begin{cases} \Pi\Gamma_{n,x}^o, x = 2^{n-l-2}, \text{ if } l \neq n-1 \\ \Pi\Gamma_{n,x}^e, x = 0, \text{ if } l = n-1, \end{cases} \quad U_j = \begin{cases} I, \text{ if } \sigma = X, \tau = I \\ S, j = l+1, \text{ if } \sigma = Y, \tau = I \\ H, j \neq l+1, \text{ if } \tau = Z \end{cases}$$

for $H = H_1$;

$$P = \begin{cases} \Pi\Gamma_{n,x}^o, x = 2^{n-l-3} + 2^{n-l-2}, \text{ if } l \neq n-2 \\ \Pi\Gamma_{n,x}^e, x = 1, \text{ if } l = n-2, \end{cases} \quad U_j = \begin{cases} I_2, \text{ if } \sigma = X, \tau = I \\ S, j \in \{l+1, l+2\} \text{ if } \sigma = Y, \tau = I \\ H, j \notin \{l+1, l+2\} \text{ if } \tau = Z \end{cases}$$

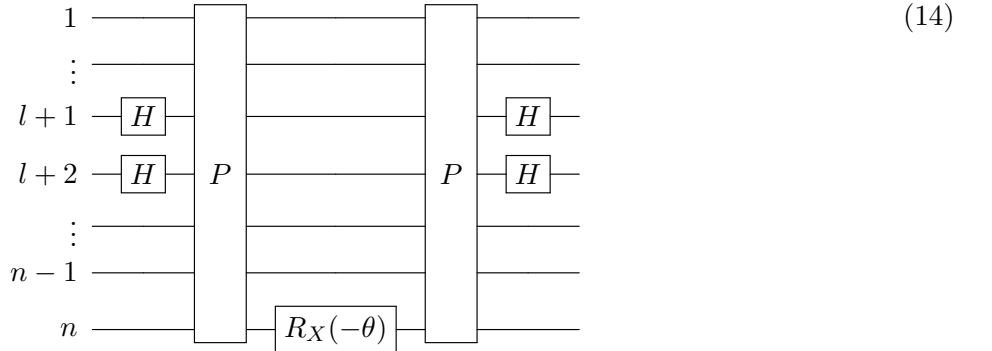
for $H = H_2$; and

$$P = \begin{cases} \Pi\Gamma_{n,x}^o, x = 0, \end{cases} \quad U_j = \begin{cases} I, \text{ if } \sigma = X, \tau = I \\ S, j = n \text{ if } \sigma = Y, \tau = I \\ H, j \neq n \text{ if } \tau = Z \end{cases}$$

for $H = H_3$. Here $1 \leq j \leq n$.

Proof: The proof follows from Algorithm 1. □

Further, if $\sigma = Z$ in Theorem 5.1 then the local Hamiltonian operators represent diagonal matrices and the unitary evolution of such Hamiltonian operators is given by us in [54] or one can just follow Algorithm 1. Following Algorithm 1, the quantum circuit for the exponential of local Hamiltonian of \mathcal{H}_{IM} i.e. $I^{\otimes l} \otimes Z \otimes Z \otimes I^{\otimes n-l-2}, l \in \{0, \dots, n-2\}$ i.e. $\exp(-i\theta I^{\otimes l} \otimes Z \otimes Z \otimes I^{\otimes n-l-2})$ is



where $P = \Pi\Gamma_{n,x}^o$ if $x = 2^{n-l-2} + 2^{n-l-3}$ if $0 \leq l < n-2$ and $P = \Pi\Gamma_{n,x}^e, x = 1$ if $l = n-2$.

Now since the local Hamiltonian operators corresponding to \mathcal{H}_{IM} are Pauli-strings formed by Kronecker product of I and Z , the quantum circuit simulation of \mathcal{H}_{IM} can be performed using these circuit models.

5.1.1 Circuit simulation with constant circuit depth for \mathcal{H}_{IM} and \mathcal{H}_{Bldg}

In this section, we illustrate that a circuit of *constant* depth can be realised through our proposed quantum circuit formulation for the unitary evolution corresponding to a 1-sparse and 2-sparse Hamiltonian operators. Recall that depth of a quantum circuit is a measurement of the number of “layers” of quantum gates that must operate concurrently to complete the computation through the circuit (Section 3.2).

From the mathematical expression of quantum Ising model given by

$$H_{\text{IM}} = \sum_{l=1}^{n-1} J_{l,l+1} Z_l Z_{l+1}$$

it is evident that all local Hamiltonian operators along with their matrix exponential commute with each other on account of being diagonal matrices. Hence,

$$\exp(-\iota H_{\text{IM}} T) = \left(\exp(-\iota H_{\text{IM}} \frac{T}{r}) \right)^r = \left(\prod_{l=1}^{n-1} \exp\left(-\iota J_{l,l+1} Z_l Z_{l+1} \frac{T}{r}\right) \right)^r = \left(\prod_{l=1}^{n-1} \exp(-\iota J_{l,l+1} Z_l Z_{l+1} T) \right)$$

Hence, in the quantum circuits of the Pauli-strings corresponding to diagonal matrices as given by equation (14), one must change the angle of the rotation gate $R_Z(J_{l,l+1} \frac{T}{r})$ in the first step to $R_Z(k J_{l,l+1} \frac{T}{r})$ in the k -th time step to $R_Z(J_{l,l+1} T) = R_Z(r J_{l,l+1} \frac{T}{r})$ in the final step. We perform this procedure for every exponential of the local Hamiltonian operator in \mathcal{H}_{IM} instead of increasing the number of layers, which provides us with a fixed depth quantum circuit.

For 2 sparse Hamiltonian $H_{\text{BLKDG}} = \sum_{\sigma \in \{I, X, Y\}} Z^{\otimes n-1} \otimes \sigma$, we see that $Z^{\otimes n-1} \otimes I$ commutes with $Z^{\otimes n-1} \otimes X + Z^{\otimes n-1} \otimes Y$. Hence,

$$\begin{aligned} \exp(-\iota H_{\text{BLKDG}} T) &= \left(\exp\left(-\iota H_{\text{BLKDG}} \frac{T}{r}\right) \right)^r \\ &= \left(\exp\left(-\iota (Z^{\otimes n-1} \otimes I) \frac{T}{r}\right) \exp\left(-\iota (Z^{\otimes n-1} \otimes (X + Y)) \frac{T}{r}\right) \right)^r \end{aligned}$$

Using standard properties of matrix exponential, we obtain

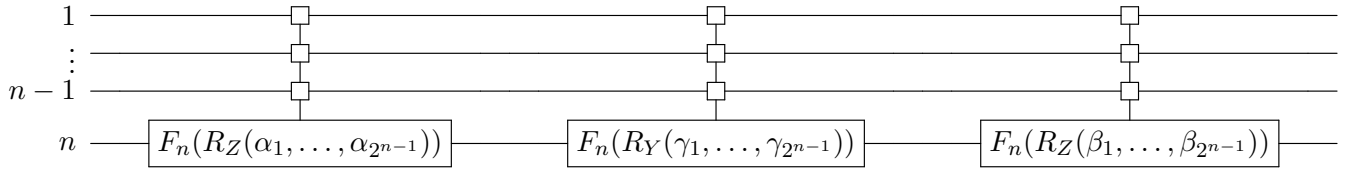
$$\exp(-\iota H_{\text{BLKDG}} T) = \underbrace{\left(\exp(-\iota (Z^{\otimes n-1} \otimes I) T) \right)}_{\text{diagonal part}} \left(\exp\left(-\iota (Z^{\otimes n-1} \otimes (X + Y)) \frac{T}{r}\right) \right)^r$$

Following [54] [55], note that $\exp(-i(Z^{\otimes n-1} \otimes (X + Y)) \frac{T}{r})$ is a block-diagonal special unitary matrix with 2×2 special unitary blocks given by

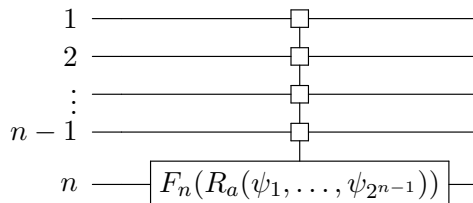
$$\begin{bmatrix} U_1(\Theta_1) & 0 & 0 & 0 \\ 0 & 0 & \ddots & 0 \\ 0 & 0 & 0 & U_{2^{n-1}}(\Theta_{2^{n-1}}) \end{bmatrix},$$

where $\Theta_j = (\alpha_j, \beta_j, \gamma_j)$ and $U_j \in SU(2)$, $j \in \{1, 2, \dots, 2^{n-1}\}$.

Moreover, the circuit for $(\exp(-i(Z^{\otimes n-1} \otimes (X + Y)) \frac{T}{r}))$ is given by



where the parameters are obtained from ZYZ decomposition of each block such that



is the multi-controlled rotation gate on an n qubit system representing the matrix

$$\left[\begin{array}{c|c|c|c} R_a(\psi_1) & 0 & 0 & 0 \\ \hline 0 & 0 & \ddots & 0 \\ \hline 0 & 0 & 0 & R_a(\psi_{2^n-1}) \end{array} \right], a \in \{Y, Z\}.$$

Hence, for each time-step, the parameter vector Θ_j changes and hence, one can accordingly change $\alpha_j, \beta_j, \gamma_j$ instead of increasing the number of layers in the circuit. Similarly for the diagonal part, using Algorithm1, one can just change the rotation gate angle of $R_X\left(\frac{T}{r}\right)$ to $R_X\left(\frac{kT}{r}\right)$ depending on the step number k . In this way, H_{BLKSDG} produces constant depth circuits for Hamiltonian simulation. Due to this phenomena, Trotter approximation error is not introduced in our circuit while writing the time-evolution unitary. Figure 2 (a) provides the quantum Ising Hamiltonian simulation and Fig-2 (b) the 2-sparse Hamiltonian simulation following the circuit approach (Section 5.1) with time measured in units of \hbar . Following Equation-8, the time evolution spans from 0 to $T = 1.0$, with each time step set at $\frac{T}{r} = 0.001$. As both of the Hamiltonian operators contain commutative relationships amongst local Hamiltonian, the Trotter decomposition following Equation (8) is exact making the Trotter error zero. The errors in Figure 2 represent the surface plot of Frobenius norm distance between the actual unitary corresponding to the Hamiltonian and the unitary obtained through the circuit model.

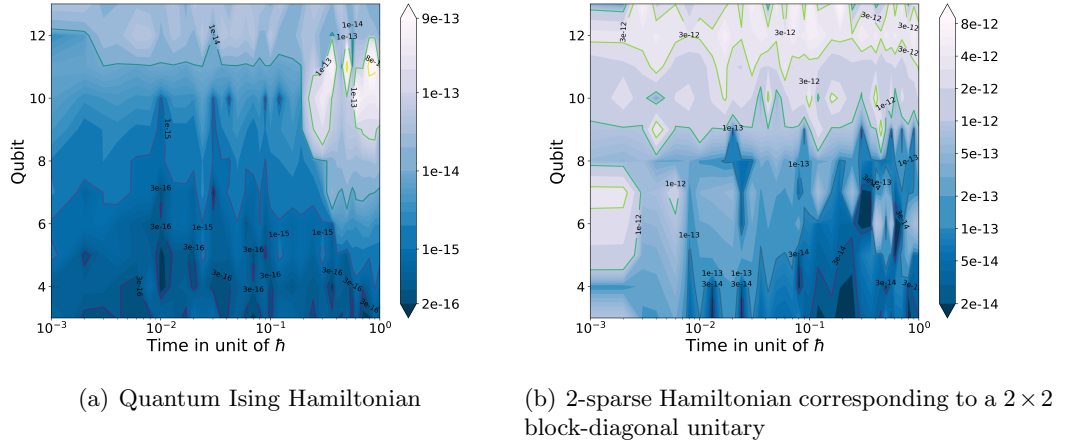


Figure 2: Surface plot of circuit simulation error for fixed depth Hamiltonian simulation of 1-sparse Quantum Ising Hamiltonian and 2-sparse Hamiltonian corresponding to a 2×2 block-diagonal unitary respectively, where the time measured in units of \hbar . The time evolution spans $T = 1.0$, with each time step set at $t = 0.001$. The error is quantified as the Frobenius norm. We observe that the error value rises with an increase in n .

5.1.2 Circuit simulation of time-independent and time-dependent \mathcal{H}_{HEIS} and \mathcal{H}_{TFQIM}

In this section, we demonstrate the quantum circuit approximation error measured in Frobenius norm distance for the unitary evolution corresponding to \mathcal{H}_{HEIS} and \mathcal{H}_{TFQIM} for both time-independent and time-dependent cases. Since the local Hamiltonian operators are 1-sparse matrices, their individual Frobenius norm attains at a very low value of order $O(10^{-16})$ to $O(10^{-12})$. Thus during the time evolution while Trotter decomposition is implemented, the total Hamiltonian simulation

error using the circuit approach closely mirrors the numerical Trotter decomposition error, which is represented by dotted lines alongside the circuit method in Figures 3, 4.

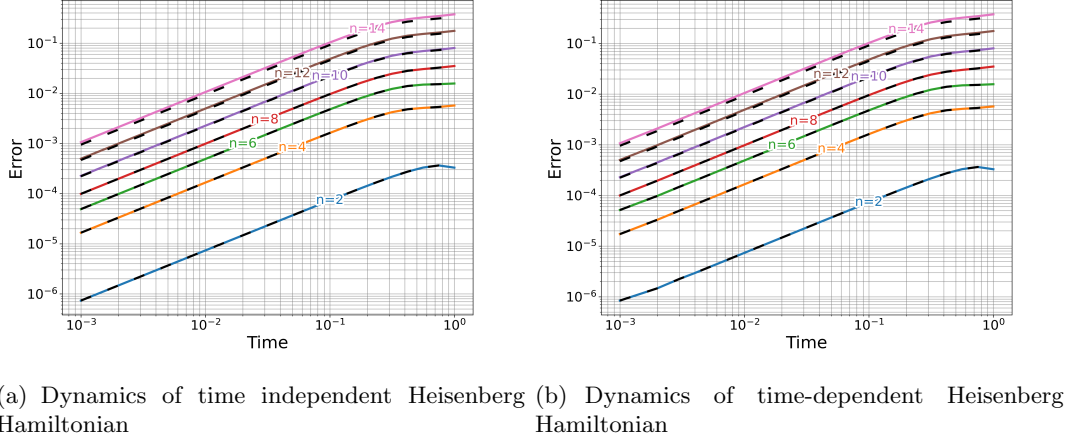


Figure 3: Line plot of circuit simulation error for Random field Heisenberg Hamiltonian for the time-independent and time-dependent case. Time is measured in units of \hbar . The time evolution spans $T = 1.0$, with each time step set at $\frac{T}{r} = 0.001$.

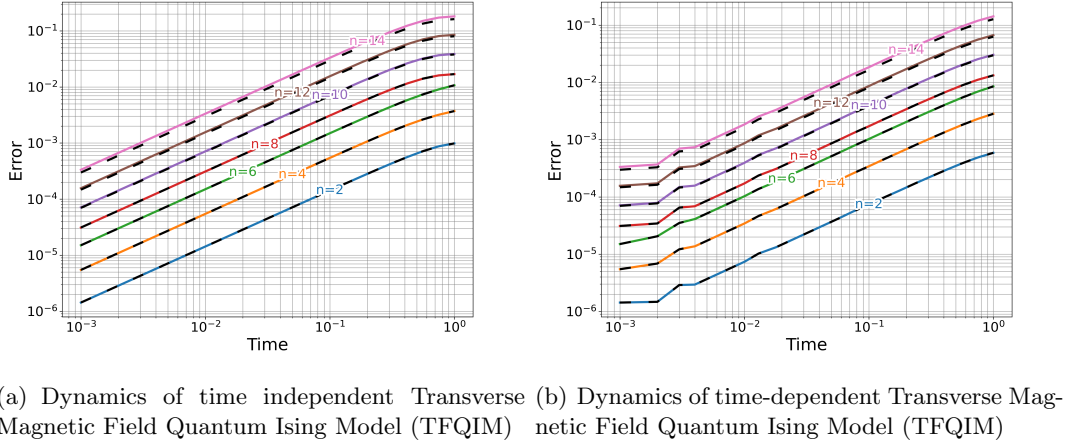


Figure 4: Line plot for Hamiltonian simulation of the Transverse Magnetic Field Quantum Ising Model (TFQIM) with random field using the Trotter product formula, both in the time-independent and time-dependent cases. Time is measured in units of \hbar . The time evolution spans $T = 1.0$, with each time step set at $\frac{T}{r} = 0.001$.

In Figure 3, we illustrate the simulations for both the time-independent (equations (4)) and time-dependent (equations (5)) Heisenberg Hamiltonian \mathcal{H}_{HEIS} respectively. In the time-independent scenario, we set $J = 1$. The time-dependent parameter $g(t)$ is defined as $\sin \frac{\omega(t)\pi}{2}$, where $\omega(t)$ takes the values 1 or -1 based on whether the time steps are even or odd during unitary evolution. Time is expressed in units of \hbar , and the time evolution spans $T = 1.0$, with each time step set at $\frac{T}{r} = 0.001$.

Similarly, in Figure 4, we simulate both time-dependent and time-independent Hamiltonian

$\mathcal{H}_{TFQIM}(t)$ as mentioned in equations (6) and (7) respectively. For the time-independent case, we shall consider J to be constant and equal to 1 and $g = \frac{J}{2}$. In the time-independent scenario, we consider J as a constant equal to 1, and set g to $\frac{J}{2}$. The time-dependent parameters $J(t)$ oscillate between 1 and 0 during even and odd time steps, and while $g(t)$ is set to be $\frac{1}{2}$.

6 Noisy simulation

NISQ systems have constraints because of short qubit decoherence times and high gate error rates. As a result, one key challenge in running simulations on current quantum hardware is preserving the distinguishability of circuit results in the presence of random noise. To demonstrate the effectiveness of our methodologies in the presence of noise, this section will describe our approach to simulating noisy circuits, incorporating two types of gate errors and two types of idle errors. The mathematical intricacies of these error channels are elaborated upon in Section 3.3. The strength of each error channel, governed by the error probability p in the descriptions of Kraus operators in Section 3.3, is chosen at random from a uniform distribution. Furthermore, in our simulation, the strength of the noise is classified into three categories: low strength, with p values ranging from 0 to 10^{-3} ; medium strength, where p lies between 10^{-3} to 10^{-1} ; and high strength, where the p spans from 10^{-1} to 10^0 . To quantify the effect of noise, the primary metric of concern is the mean fidelity $\mathcal{F}(t)$, which measures the distance between the ideal (noise-free) and noisy output state vectors by calculating their squared overlap. Indeed, let $|\psi(t)\rangle$ and $|\psi(t)\rangle_{ns}$ denote the quantum states after time t when $|\psi(0)\rangle$ is evolved using a noiseless and noisy circuit respectively. Then the fidelity [4] between $|\psi(t)\rangle$ and $|\psi(t)\rangle_{ns}$ is defined as

$$\mathcal{F}(t) = |\langle \psi(t) | \psi(t) \rangle_{ns}|^2. \quad (15)$$

Now using the Kraus operator formalism [29], we perform the noisy circuit simulation with the initial states $(H|0\rangle)^{\otimes n} = ((|0\rangle + |1\rangle)/\sqrt{2})^{\otimes n}$ and $|1\rangle^{\otimes n}$. Figure 5, 6 depict the results of these simulations under various scenarios: 1. Low gate and idle error strengths, 2. Low gate error but high idle error strengths (and vice versa), 3. High gate and idle error strengths, and 4. Medium gate and idle error strengths. In this context, 'low,' 'medium,' and 'high' denote the error strengths discussed in Section 3.3. Gate errors encompass both bit-flip and phase-flip errors, while idle errors encompass both amplitude damping and phase damping. The strength of noise channels is classified into three categories: low strength, with values ranging from 0 to 10^{-3} ; medium strength, where values lie between 10^{-3} to 10^{-1} ; and high strength, where the value spans from 10^{-1} to 10^0 .

In Figures 5, 6 we observe the influence of the error in the quantum circuit and the input state, while calculating the fidelity of the quantum state after passing through the noiseless and noisy quantum channel during time evolution. We note that when both gate and idle noise strength are low, the fidelity remains close to 1 irrespective of the input state. Conversely, under other conditions—such as when either the gate or idle noise strength is medium, or when one is high while the other is low (or vice versa), or when both are high—we observe a deterioration in fidelity for the noisy quantum channel, particularly when the input state is $((|0\rangle + |1\rangle)/\sqrt{2})^{\otimes n}$ compared to $|1\rangle^{\otimes n}$. Additionally, regardless of the input state, we find that when both gate and idle noise strengths are medium, the fidelity notably improves compared to the latter two scenarios where one (or both) of the gate and idle noise strengths are high. Only in Figure 5, we observe that with the input state $|1\rangle^{\otimes n}$, the fidelity value $\mathcal{F}(t)$ for low gate and high idle noise strength surpasses the other two cases that are high gate and low (or high) idle noise strength. However, the fidelity value is deemed unacceptable for all other cases.

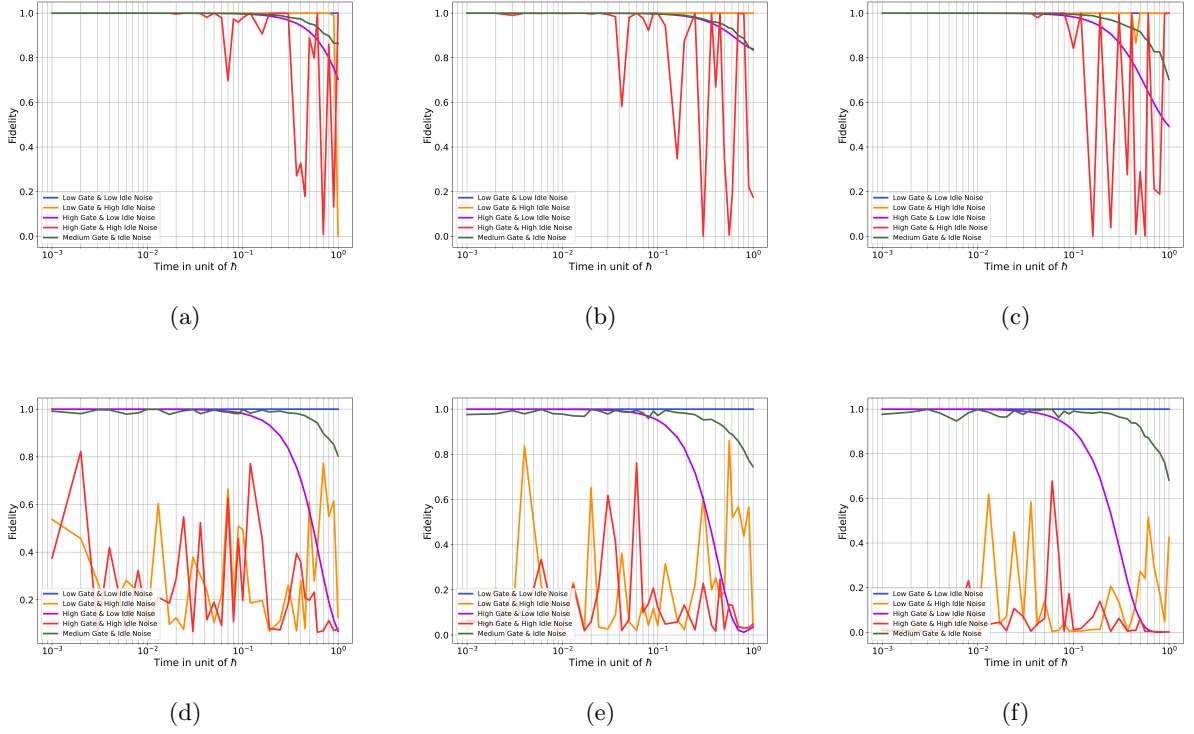


Figure 5: Fidelity $\mathcal{F}(t)$ between quantum states after passing through the noiseless and noisy circuit as a function of time and error strength for time-independent Random Field Heisenberg Hamiltonian. Figures (a), (b), (c) are with input state $|\psi(0)\rangle = |1\rangle^{\otimes n}$ for 4, 6 and 8 qubits respectively, whereas Figures (d), (e), (f) are with input state $|\psi(0)\rangle = (|0\rangle + |1\rangle)/\sqrt{2}^{\otimes n}$ for 4, 6 and 8 qubits respectively.

Conclusion. In this paper, we propose a scalable quantum circuit implementation of Pauli-string exponential that are suitable for digital quantum computation. The circuits are defined by one-qubit gates and CNOT gates, which favors its implementation in a star-like quantum hardware efficiently exploiting a permutation similarity of string of X gates. Then these circuits are employed to simulate several time-independent and time-dependent 1D Hamiltonian operators by approximating its evolution using first-order Suzuki-Trotter product formula. Indeed, it must be noted that the proposed methodology can be used for any other decomposition methods such as *second-order symmetric Trotter formula* and *order $2k$ symmetric Suzuki-Trotter formula*. Simulations involving up to 14 qubits demonstrate that the error from the proposed circuit model simulation of Hamiltonian operators closely matches the numerical Trotter approximation error across all cases. Additionally, we observe that circuits of constant depth can handle the evolution of 1-sparse Hamiltonian and 2-sparse Ising Hamiltonian. Finally, we incorporate various noise models for gate errors and idle errors to assess the efficiency of the circuit models in NISQ computers for systems of up to 8 qubits governed by time-independent Random Field Heisenberg Hamiltonian and time-independent transverse magnetic random quantum Ising models. These simulations show that the value of the fidelity $\mathcal{F}(t)$ between the outputs for noisy and noiseless simulation drops down to the 0.8 mark during the end of the time evolution for certain states when the magnitude of gate error and idle error ranges between 10^{-3} to 10^{-1} for different input states. Besides, when the evolution time is near to zero the value $1 - \mathcal{F}(t) < 10^{-4}$ regardless of the input states. Finally, it is evident that the selection of the input

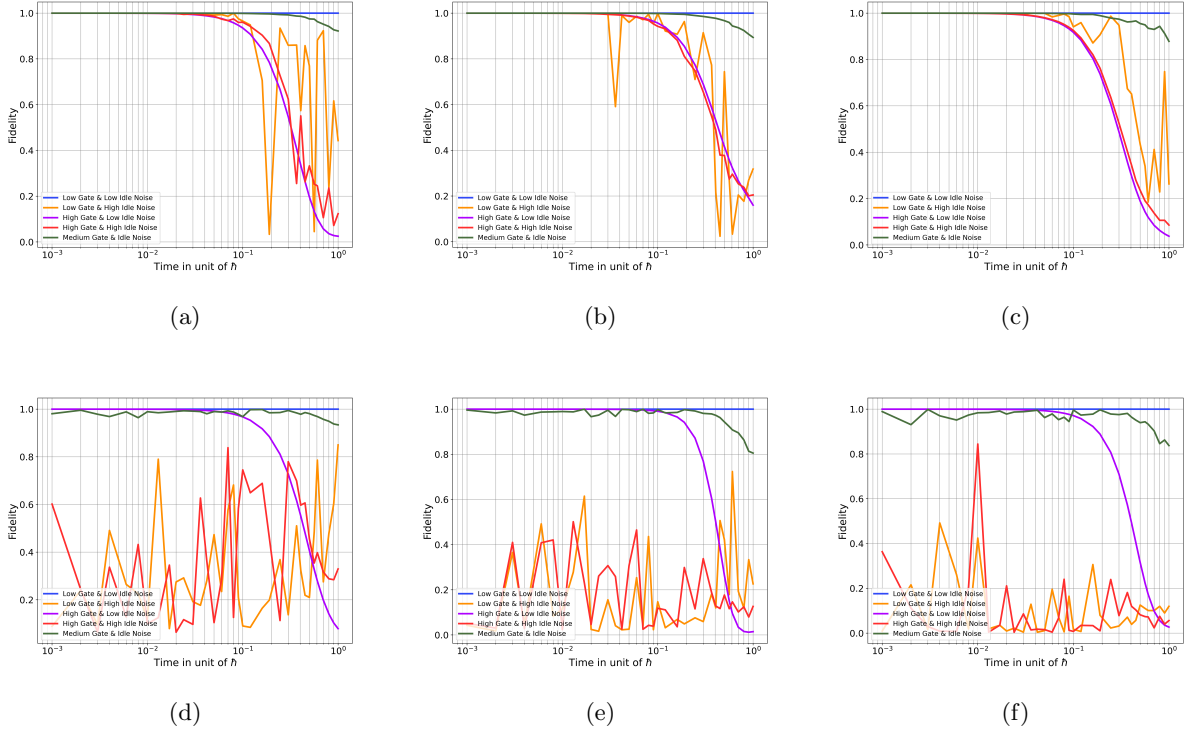


Figure 6: Fidelity $\mathcal{F}(t)$ between quantum states after passing through the noiseless and noisy circuit as a function of time and error strength for time-independent transverse magnetic random quantum Ising model \mathcal{H}_{TFQIM} . Figures (a), (b), (c) are with input state $|1\rangle^{\otimes n}$ for 4, 6 and 8 qubits respectively, whereas Figures (d), (e), (f) are with input state $(|0\rangle + |1\rangle)/\sqrt{2}^{\otimes n}$ for 4, 6 and 8 qubits respectively.

state holds significant importance in noisy simulations.

We emphasize that our proposed circuit model for Hamiltonian simulation does not involve partitioning the set of Pauli-strings of the Hamiltonian operators into commutative and non-commutative clusters, which presents a separate challenging problem. Such partitioning has the potential to decrease the number of quantum gates in the circuit. We explore this aspect in our future work.

Acknowledgement: RSS and SC acknowledge support through Prime Minister’s Research Fellowship (PMRF), Government of India.

References

- [1] Boris Arseniev, Dmitry Guskov, Richik Sengupta, and Igor Zacharov. Tridiagonal matrix decomposition for hamiltonian simulation on a quantum computer. *arXiv preprint arXiv:2310.00121*, 2024.
- [2] Stefan Backens, Alexander Shnirman, and Yuriy Makhlin. Jordan–wigner transformations for tree structures. *Scientific reports*, 9(1):2598, 2019.

- [3] Marcello Benedetti, Mattia Fiorentini, and Michael Lubasch. Hardware-efficient variational quantum algorithms for time evolution. *Physical Review Research*, 3(3):033083, 2021.
- [4] Ingemar Bengtsson and Karol Życzkowski. *Geometry of quantum states: an introduction to quantum entanglement*. Cambridge university press, 2017.
- [5] Dominic W Berry, Andrew M Childs, Richard Cleve, Robin Kothari, and Rolando D Somma. Simulating hamiltonian dynamics with a truncated taylor series. *Physical review letters*, 114(9):090502, 2015.
- [6] Kishor Bharti, Alba Cervera-Lierta, Thi Ha Kyaw, Tobias Haug, Sumner Alperin-Lea, Abhinav Anand, Matthias Degroote, Hermann Heimonen, Jakob S Kottmann, Tim Menke, et al. Noisy intermediate-scale quantum algorithms. *Reviews of Modern Physics*, 94(1):015004, 2022.
- [7] Earl Campbell. Random compiler for fast hamiltonian simulation. *Physical review letters*, 123(7):070503, 2019.
- [8] Andrew M Childs, Dmitri Maslov, Yunseong Nam, Neil J Ross, and Yuan Su. Toward the first quantum simulation with quantum speedup. *Proceedings of the National Academy of Sciences*, 115(38):9456–9461, 2018.
- [9] Andrew M Childs, Aaron Ostrander, and Yuan Su. Faster quantum simulation by randomization. *Quantum*, 3:182, 2019.
- [10] Andrew M Childs and Yuan Su. Nearly optimal lattice simulation by product formulas. *Physical review letters*, 123(5):050503, 2019.
- [11] Andrew M. Childs, Yuan Su, Minh C. Tran, Nathan Wiebe, and Shuchen Zhu. Theory of trotter error with commutator scaling. *Phys. Rev. X*, 11:011020, Feb 2021.
- [12] Andrew M. Childs and Nathan Wiebe. Hamiltonian simulation using linear combinations of unitary operations. *Quantum Information and Computation*, 12(11 & 12):901–924, November 2012.
- [13] Laura Clinton, Johannes Bausch, and Toby Cubitt. Hamiltonian simulation algorithms for near-term quantum hardware. *Nature Communications*, 12(1):4989, 2021.
- [14] IBM Q experience backend information. <https://github.com/dcmckayibm/ibmqx-backend-information>, 2017.
- [15] PARAM Shakti High Performance Computing Facility. <http://www.hpc.iitkgp.ac.in/hpcf/paramshakti>.
- [16] Paul K Faehrmann, Mark Steudtner, Richard Kueng, Maria Kieferova, and Jens Eisert. Randomizing multi-product formulas for hamiltonian simulation. *Quantum*, 6:806, 2022.
- [17] Benedikt Fauseweh. Quantum many-body simulations on digital quantum computers: State-of-the-art and future challenges. *Nature Communications*, 15(1):2123, 2024.
- [18] Patrik Fazekas. *Lecture notes on electron correlation and magnetism*, volume 5. World scientific, 1999.

- [19] Pranav Gokhale, Olivia Angiuli, Yongshan Ding, Kaiwen Gui, Teague Tomesh, Martin Suchara, Margaret Martonosi, and Frederic T Chong. Minimizing state preparations in variational quantum eigensolver by partitioning into commuting families. *arXiv preprint arXiv:1907.13623*, 2023.
- [20] David Gosset, Vadym Kliuchnikov, Michele Mosca, and Vincent Russo. An algorithm for the t-count. *arXiv preprint arXiv:1308.4134*, 2013.
- [21] Jeongwan Haah, Matthew B Hastings, Robin Kothari, and Guang Hao Low. Quantum algorithm for simulating real time evolution of lattice hamiltonians. *SIAM Journal on Computing*, (0):FOCS18–250, 2021.
- [22] Naomichi Hatano and Masuo Suzuki. Finding exponential product formulas of higher orders. *Quantum annealing and other optimization methods*, pages 37–68, 2005.
- [23] Walter Hofstetter and Tao Qin. Quantum simulation of strongly correlated condensed matter systems. *Journal of Physics B: Atomic, Molecular and Optical Physics*, 51(8):082001, 2018.
- [24] Yoshiaki Kawase and Keisuke Fujii. Fast classical simulation of hamiltonian dynamics by simultaneous diagonalization using clifford transformation with parallel computation. *Computer Physics Communications*, 288:108720, 2023.
- [25] Alastair Kay. Quantum error correction for state transfer in noisy spin chains. *Physical Review A*, 93(4):042320, 2016.
- [26] Mária Kieferová, Artur Scherer, and Dominic W Berry. Simulating the dynamics of time-dependent hamiltonians with a truncated dyson series. *Physical Review A*, 99(4):042314, 2019.
- [27] M Kjaergaard, ME Schwartz, A Greene, GO Samach, A Bengtsson, M O’Keeffe, CM McNally, J Braumüller, DK Kim, P Krantz, et al. Demonstration of density matrix exponentiation using a superconducting quantum processor. *Physical Review X*, 12(1):011005, 2022.
- [28] Alexander Klein and Dieter Jaksch. Simulating high-temperature superconductivity model hamiltonians with atoms in optical lattices. *Physical Review A*, 73(5):053613, 2006.
- [29] Karl Kraus, Arno Böhm, John D Dollard, and WH Wootters. *States, Effects, and Operations Fundamental Notions of Quantum Theory: Lectures in Mathematical Physics at the University of Texas at Austin*. Springer, 1983.
- [30] Tomochika Kurita, Mikio Morita, Hirotaka Oshima, and Shintaro Sato. Pauli string partitioning algorithm with the ising model for simultaneous measurements. *The Journal of Physical Chemistry A*, 127(4):1068–1080, 2023.
- [31] Benjamin P Lanyon, James D Whitfield, Geoff G Gillett, Michael E Goggin, Marcelo P Almeida, Ivan Kassal, Jacob D Biamonte, Masoud Mohseni, Ben J Powell, Marco Barbieri, et al. Towards quantum chemistry on a quantum computer. *Nature chemistry*, 2(2):106–111, 2010.
- [32] Jonathan Wei Zhong Lau, Tobias Haug, Leong Chuan Kwek, and Kishor Bharti. NISQ Algorithm for Hamiltonian simulation via truncated Taylor series. *SciPost Physics*, 12:122, 2022.
- [33] Gushu Li, Yufei Ding, and Yuan Xie. Tackling the qubit mapping problem for nisq-era quantum devices. In *Proceedings of the Twenty-Fourth International Conference on Architectural Support for Programming Languages and Operating Systems*, pages 1001–1014, 2019.

- [34] Phillip C. Lotshaw, Hanjing Xu, Bilal Khalid, Gilles Buchs, Travis S. Humble, and Arnab Banerjee. Simulations of frustrated ising hamiltonians using quantum approximate optimization. *Philosophical Transactions of the Royal Society A: Mathematical, Physical and Engineering Sciences*, 381(2241):20210414, 2023.
- [35] Guang Hao Low and Isaac L Chuang. Optimal hamiltonian simulation by quantum signal processing. *Physical review letters*, 118(1):010501, 2017.
- [36] Guang Hao Low and Isaac L Chuang. Hamiltonian simulation by qubitization. *Quantum*, 3:163, 2019.
- [37] Guang Hao Low and Nathan Wiebe. Hamiltonian simulation in the interaction picture. *arXiv preprint arXiv:1805.00675*, 2018.
- [38] M. Mansky, V. Puigvert, Castillo S., and C. Linnhoff-Popien. Decomposition algorithm of an arbitrary pauli exponential through a quantum circuit. In *2023 IEEE International Conference on Quantum Computing and Engineering (QCE)*, pages 434–442, Los Alamitos, CA, USA, 2023. IEEE Computer Society.
- [39] Norman H March and Giuseppe GN Angilella. *Exactly solvable models in many-body theory*. World Scientific, 2016.
- [40] Sam McArdle, Suguru Endo, Alán Aspuru-Guzik, Simon C Benjamin, and Xiao Yuan. Quantum computational chemistry. *Reviews of Modern Physics*, 92(1):015003, 2020.
- [41] Priyanka Mukhopadhyay, Nathan Wiebe, and Hong Tao Zhang. Synthesizing efficient circuits for hamiltonian simulation. *npj Quantum Information*, 9, 2023.
- [42] Michael A Nielsen and Isaac L Chuang. *Quantum computation and quantum information*. Cambridge university press, 2010.
- [43] Johann Ostmeier. Optimised trotter decompositions for classical and quantum computing. *Journal of Physics A: Mathematical and Theoretical*, 56(28):285303, 2023.
- [44] Bo Peng, Sahil Gulania, Yuri Alexeev, and Niranjana Govind. Quantum time dynamics employing the yang-baxter equation for circuit compression. *Phys. Rev. A*, 106:012412, Jul 2022.
- [45] Sebastiano Peotta, Fredrik Brange, Aydin Deger, Teemu Ojanen, and Christian Flindt. Determination of dynamical quantum phase transitions in strongly correlated many-body systems using loschmidt cumulants. *Physical Review X*, 11(4):041018, 2021.
- [46] Antonio Sergio Teixeira Pires. *Theoretical tools for spin models in magnetic systems*. IOP Publishing, 2021.
- [47] David Poulin, Angie Qarry, Rolando Somma, and Frank Verstraete. Quantum simulation of time-dependent hamiltonians and the convenient illusion of hilbert space. *Physical review letters*, 106(17):170501, 2011.
- [48] Qiskit contributors. Qiskit: An open-source framework for quantum computing, 2023,10.5281/zenodo.2573505.
- [49] IBM Quantum. Quantum circuits — IBM Quantum Documentation — docs.quantum.ibm.com. <https://docs.quantum.ibm.com/api/qiskit/circuit>. [Accessed 28-02-2024].

- [50] Sadegh Raeisi, Nathan Wiebe, and Barry C Sanders. Quantum-circuit design for efficient simulations of many-body quantum dynamics. *New Journal of Physics*, 14:103017, 2023.
- [51] Markus Reiher, Nathan Wiebe, Krysta M. Svore, Dave Wecker, and Matthias Troyer. Elucidating reaction mechanisms on quantum computers. *Proceedings of the National Academy of Sciences*, 114(29):7555–7560, 2017.
- [52] Gumaro Rendon, Jacob Watkins, and Nathan Wiebe. Improved accuracy for trotter simulations using chebyshev interpolation. *Quantum*, 8:1266, 2024.
- [53] Angel Rivas and Susana F Huelga. *Open quantum systems*, volume 10. Springer, 2012.
- [54] Rohit Sarma Sarkar and Bibhas Adhikari. Scalable quantum circuits for n-qubit unitary matrices. In *2023 IEEE International Conference on Quantum Computing and Engineering (QCE)*, volume 01, pages 1078–1088, 2023.
- [55] Rohit Sarma Sarkar and Bibhas Adhikari. A quantum neural network framework for scalable quantum circuit approximation of unitary matrices. *arXiv preprint arXiv:2405.00012*, 2024.
- [56] Jinjing Shi, Wenxuan Wang, Xiaoping Lou, Shichao Zhang, and Xuelong Li. Parameterized hamiltonian learning with quantum circuit. *IEEE Transactions on Pattern Analysis and Machine Intelligence*, 45(5):6086–6095, 2022.
- [57] Ralph Skomski. *Simple models of magnetism*. Oxford university press, 2008.
- [58] Daniel Stilck França and Raul Garcia-Patron. Limitations of optimization algorithms on noisy quantum devices. *Nature Physics*, 17(11):1221–1227, 2021.
- [59] Jinzhao Sun, Suguru Endo, Huiping Lin, Patrick Hayden, Vlatko Vedral, and Xiao Yuan. Perturbative quantum simulation. *Physical Review Letters*, 129(12):120505, 2022.
- [60] Masuo Suzuki. Generalized trotter’s formula and systematic approximants of exponential operators and inner derivations with applications to many-body problems. *Communications in Mathematical Physics*, 51(2):183–190, 1976.
- [61] Masuo Suzuki. General theory of fractal path integrals with applications to many-body theories and statistical physics. *Journal of Mathematical Physics*, 32(2):400–407, 1991.
- [62] Hale F Trotter. On the product of semi-groups of operators. *Proceedings of the American Mathematical Society*, 10(4):545–551, 1959.
- [63] Ewout van den Berg and Kristan Temme. Circuit optimization of Hamiltonian simulation by simultaneous diagonalization of Pauli clusters. *Quantum*, 4:322, 2020.
- [64] Samson Wang, Enrico Fontana, Marco Cerezo, Kunal Sharma, Akira Sone, Lukasz Cincio, and Patrick J Coles. Noise-induced barren plateaus in variational quantum algorithms. *Nature communications*, 12(1):6961, 2021.
- [65] Nathan Wiebe, Christopher Granade, Christopher Ferrie, and David G Cory. Hamiltonian learning and certification using quantum resources. *Physical review letters*, 112(19):190501, 2014.

- [66] Yong-Xin Yao, Niladri Gomes, Feng Zhang, Cai-Zhuang Wang, Kai-Ming Ho, Thomas Iadecola, and Peter P Orth. Adaptive variational quantum dynamics simulations. *PRX Quantum*, 2(3):030307, 2021.
- [67] Yordan S. Yordanov, David R. M. Arvidsson-Shukur, and Crispin H. W. Barnes. Efficient quantum circuits for quantum computational chemistry. *Phys. Rev. A*, 102:062612, Dec 2020.
- [68] Xiao Yuan, Suguru Endo, Qi Zhao, Ying Li, and Simon C Benjamin. Theory of variational quantum simulation. *Quantum*, 3:191, 2019.